

# *Forecasting the monsoon on daily to seasonal time-scales in support of a field campaign*

Article

Published Version

Creative Commons: Attribution 4.0 (CC-BY)

Open Access

Martin, G. M., Brooks, M. E., Johnson, B., Milton, S. F., Webster, S., Jayakumar, A., Mitra, A. K., Rajan, D. and Hunt, K. M. R. ORCID: <https://orcid.org/0000-0003-1480-3755> (2020) Forecasting the monsoon on daily to seasonal time-scales in support of a field campaign. Quarterly Journal of the Royal Meteorological Society, 146 (731). pp. 2906-2927. ISSN 1477-870X doi: 10.1002/qj.3620 Available at <https://centaur.reading.ac.uk/90498/>

It is advisable to refer to the publisher's version if you intend to cite from the work. See [Guidance on citing](#).

Published version at: <http://dx.doi.org/10.1002/qj.3620>

To link to this article DOI: <http://dx.doi.org/10.1002/qj.3620>

Publisher: Royal Meteorological Society

All outputs in CentAUR are protected by Intellectual Property Rights law, including copyright law. Copyright and IPR is retained by the creators or other copyright holders. Terms and conditions for use of this material are defined in the [End User Agreement](#).




[www.reading.ac.uk/centaur](http://www.reading.ac.uk/centaur)

## **CentAUR**

Central Archive at the University of Reading

Reading's research outputs online

# Forecasting the monsoon on daily to seasonal time-scales in support of a field campaign

Gill M. Martin<sup>1</sup>  | Malcolm E. Brooks<sup>1</sup> | Ben Johnson<sup>1</sup> | Sean F. Milton<sup>1</sup> | Stuart Webster<sup>1</sup> | A. Jayakumar<sup>2</sup>  | Ashis K. Mitra<sup>2</sup> | D. Rajan<sup>2</sup> | Kieran M. R. Hunt<sup>3</sup> 

<sup>1</sup>Met Office, Exeter, UK

<sup>2</sup>National Center for Medium Range Weather Forecasting, Noida, India

<sup>3</sup>Department of Meteorology, University of Reading, Reading, UK

## Correspondence

Gill M. Martin, Met Office, FitzRoy Road, Exeter, EX1 3PB, UK.

Email: gill.martin@metoffice.gov.uk

## Funding information

Met Office Hadley Centre Climate Programme funded by BEIS and Defra; Natural Environment Research Council Grant Number: NE/L01386X/1; Ministry of Earth Sciences, Monsoon Mission; JPI-Climate and Belmont Forum Climate Predictability and Inter-Regional Linkages Collaborative Research Action via NERC grant NE/P006795/1.

## Abstract

The successful planning and execution of a major field campaign relies on the availability and reliability of weather forecasts on a range of time-scales. Here, we describe the wide range of forecast products generated in support of a field campaign that took place in India in 2016 as part of the Interaction of Convective Organization with Monsoon Precipitation, Atmosphere, Surface and Sea (INCOMPASS) project. We show examples of the suite of plots generated every day from the forecasts and supplied to the mission scientists, and describe how these were used to plan the flights. We highlight the benefits of having access to forecasts from a range of model resolutions and configurations; these allowed judgements to be made about uncertainty, particularly in the amount and location of deep convective rainfall, which is an important consideration for flight planning. Finally, we discuss the legacy of the forecasting activity, which has not only advanced our understanding of monsoon forecasting but also created a large database of targeted model forecast products for the whole of the 2016 monsoon season. These can be used by researchers for comparisons with in situ observations as well as future modelling studies.

## KEYWORDS

field campaign, forecast, INCOMPASS, India, monsoon

## 1 | INTRODUCTION

A major field campaign took place in India in 2016 as part of the Interaction of Convective Organization with Monsoon Precipitation, Atmosphere, Surface and Sea (INCOMPASS) project, the ultimate goal of which was better understanding and prediction of monsoon rainfall. A comprehensive set of measurements was taken over a period of one month, including airborne measurements using the UK Facility for Airborne Atmospheric Measurement (FAAM) Atmospheric Research Aircraft (ARA), ground-based observations from a

network of eddy-covariance towers, and upper-air measurement from radiosondes. A comprehensive overview of the field campaign is given in Turner *et al.* (2019).

Several successful observational campaigns involving aircraft and ground-based measurements have been carried out over India during the past few decades (e.g., Bhat and Narasimha, 2007; Kulkarni *et al.*, 2012). The successful planning and execution of a major field campaign relies on the availability and reliability of weather forecasts on a range of time-scales. Since flight plans must be filed some days in advance, researchers require timely access to forecast

This is an open access article under the terms of the Creative Commons Attribution License, which permits use, distribution and reproduction in any medium, provided the original work is properly cited.

© 2019 The Authors and Crown Copyright, Met Office. Quarterly Journal of the Royal Meteorological Society published by John Wiley & Sons Ltd on behalf of the Royal Meteorological Society

products that will allow them to work out the details of the routes and manoeuvres needed to sample the atmospheric conditions adequately.

In support of this field campaign, and particularly to assist flight planning, a range of forecast tools were employed. These were largely based on the Met Office Unified Model (MetUM) as used operationally at the Met Office and at India's National Center for Medium Range Weather Forecasting (NCMRWF). Forecast configurations ranged from global operational forecasts at 17-km resolution to convection-permitting configurations at 4.4- and 1.5-km resolution (run over a limited area 5°N–35°N, 50°E–100°E) nested within the global operational configuration. Forecast outputs in the form of a set of standard plots covering a range of key meteorological variables were examined on a daily basis in the run-up to the campaign, during the flying period, and subsequently for several weeks thereafter. Prior to the campaign, seasonal forecasts were examined in order to provide guidance as to the likely timing of monsoon onset and the pre- and postonset conditions that might be experienced during the northern and southern phases of the campaign.

In this article, we describe various aspects of the forecasting activity in order to illustrate how the use of multiple forecast products, and a day-to-day focus on the developing monsoon conditions, assisted the flight planning and subsequent understanding of the monsoon weather encountered during the campaign. During May and June of the previous year (2015), a “dry run” of the flight planning was carried out, providing the INCOMPASS team with some familiarity with the forecasting tools and allowing an optimum set of model outputs to be designed. This activity, and the characteristics of monsoon onset observed during that period, are described in Willetts *et al.* (2017a). However, to our knowledge, real-time forecasting activity in support of an active field campaign has not been documented previously in the scientific literature.

The article is arranged as follows: in sections 2 and 3 we describe the model configurations employed and the methodology used; section 4 describes the use of seasonal forecasting ahead of the campaign to anticipate the conditions that would be encountered. In section 5 we illustrate how the forecasts were used in support of flight planning, using three case studies, while in section 6 we summarize the overall benefits of the forecasting activity to the campaign. Finally, in section 7 we discuss the legacy of this activity, which includes a dataset that will be used to provide further insight that will ultimately contribute to the goal of improving monsoon forecasting on a range of time-scales.

## 2 | MODEL CONFIGURATIONS

Table 1 shows the range of model configurations used for flight planning during the INCOMPASS field campaign. The main forecasting tool for this campaign was the Met Office

Unified Model (MetUM). The operational weather forecasting model version in use in 2016 was the GA6.1/GL6.1 science configuration (Walters *et al.*, 2017), operating at a horizontal resolution of N768 (17km) with 70 vertical levels and a model lid at 80 km. The Global Atmosphere (GA) version 6.1 science configuration includes the ENDGame semi-implicit, semi-Lagrangian dynamical core (Wood *et al.*, 2014), a prognostic cloud and condensate scheme (PC2: Wilsson *et al.*, 2008), a subgrid orographic gravity-wave drag representation with flow blocking (Vosper, 2015), parametrized deep convection using a bulk mass-flux scheme developed by Gregory and Rowntree (1990) with the inclusion of downdraughts (Gregory and Allen, 1991), convective momentum transport (Stratton *et al.*, 2009) and a convective available potential energy closure scheme (Fritsch and Chappell, 1980), a shallow convection scheme (Grant and Brown, 1999; Grant, 2001), and a non-local boundary-layer scheme (Lock *et al.*, 2000) with modifications described in Lock (2001) and Brown *et al.* (2008). Global Land (GL) version 6.1 defines the global land science configuration, which uses the Joint UK Land Environment Simulator (JULES) community land surface model (Best *et al.*, 2011; Clark *et al.*, 2011). Prakash *et al.* (2016) showed good skill for five-day forecasts of the 2014 Indian monsoon season with this MetUM configuration.

In order to provide more local detail in the forecasts for the campaign, a bespoke limited-area model (LAM) was developed covering a domain of 5°N–35°N, 50°E–100°E. The LAM operated at a resolution of 4.4 km in the horizontal and also used finer vertical resolution through the troposphere, with 80 vertical levels below the 38.5-km model lid. The LAM was initialized using the interpolated global model analysis flow fields and forced at the lateral boundaries from large-scale conditions generated every hour by the global model. The differences in the science configuration of the 4.4 km LAM relative to the global model are as follows. First and foremost, this LAM represented convection explicitly, that is, the convection parametrization was completely switched off. Second, this LAM employs a diagnostic (rather than a prognostic) subgrid cloud scheme (Smith, 1990), which diagnoses the liquid cloud fraction and condensed water when the grid-box mean relative humidity exceeds a critical value ( $RH_{crit}$ ) that is 96% in the lowest model level, decreases gradually over 15 model levels to 80% by 1 km above the surface, and is constant throughout the profile thereafter. Third, subgrid turbulence is represented by a “blended” boundary-layer parametrization (Boutle *et al.*, 2014) in which, depending on the diagnosed boundary-layer depth, the subgrid mixing is a proportion of that predicted by the 1D global scheme combined with a proportion of that predicted by the Smagorinsky 3D turbulence scheme (Smagorinsky, 1963). Finally, one relatively new feature included in this LAM configuration was the use of a moisture conservation scheme (Aranami *et al.*, 2015), with the moisture within the LAM domain being conserved

TABLE 1 Model configurations used in support of the INCOMPASS field campaign. See text for details

Model	Documentation	Resolution	Levels	Lid	Convection scheme	PBL scheme	Cloud scheme	Model time step	LBC update frequency	Forecast length
GloSea5	MacLachlan <i>et al.</i> (2015)	N216 (0.83°×0.56°), ORCA0.25 (0.25°×0.25°)	85	85 km	Mass flux convection scheme	Unstable PBL scheme	Prognostic	15 min	N/A	210 days
MetUM global	Walters <i>et al.</i> (2017)	N768 (0.234°×0.16°)	70	80 km	Mass flux convection scheme	Unstable PBL scheme	Prognostic	7.5 min	N/A	7 days
NCUM global	Rakhi <i>et al.</i> (2016), George <i>et al.</i> (2016b)	N768 (0.234°×0.16°)	70	80 km	Mass flux convection scheme	Unstable PBL scheme	Prognostic	7.5 min	N/A	10 days
GA6 + memory	Willett and Whittall (2017), Walters <i>et al.</i> (2017)	0.234°×0.16° nested in global	70	80 km	Mass flux scheme with convective memory	Unstable PBL scheme	Prognostic	7.5 min	1 hr	2.5 days
GA6 + CLASSIC	Bellouin <i>et al.</i> (2011), Walters <i>et al.</i> (2017)	0.234°×0.16° nested in global	70	80 km	Mass flux convection scheme	Unstable PBL scheme	Prognostic	7.5 min	1 hr	2.5 days
MetUM LAM	Stratton <i>et al.</i> (2018)	4.4 km	80	38.5 km	Off	Blended PBL scheme with mixing factor 0.5	Diagnostic	100 s	1 hr	2.5 days
NCMRWF LAM 4 km	Mamgain <i>et al.</i> (2018)	4 km	80	38.5 km	Off	Blended PBL scheme with mixing factor 0.5	Diagnostic	1 min	1 hr	3.125 days
NCMRWF LAM 1.5 km	Jayakumar <i>et al.</i> (2017)	1.5 km	80	38.5 km	Off	Blended PBL scheme with mixing factor 0.5	Diagnostic	1 min	1 hr	3.125 days

appropriately by ensuring that the mass flux through the lateral boundaries was accounted for in the budget calculation. The impact of this scheme was most evident for localized convection, with a reduction in excessive rainfall amounts when the scheme was included. A more comprehensive description of the 4.4-km LAM configuration used here, and its benefits to the simulation of tropical rainfall, can be found in Stratton *et al.* (2018) and Woodhams *et al.* (2018).

In addition, two further models were run for research purposes. The first of these, termed “GA6+memory”, used the same resolution as the global model and was nested in the global operational configuration. The physics configuration was the same as in the operational global model, except for the use of an experimental convection parametrization that included a representation of convective “memory” through the use of a prognostic-based entrainment rate (Willett and Whittall, 2017). This is intended to improve the spatial and temporal organization of convection by allowing locations that have experienced high levels of recent convective activity to be populated by relatively large convective clouds with low entrainment rates, and locations that have experienced low levels of recent activity to be populated by relatively small convective clouds (if any) with high entrainment rates. Willett and Whittall (2017) showed that the scheme is able to improve some aspects of tropical variability, particularly the diurnal cycle and precipitation intensity, whilst maintaining, or in some cases improving, the mean climate and forecast performance.

The second research model was an exact copy of the operational global forecast model, but with the addition of a simplified version of the Coupled Large-scale Aerosol Scheme for Simulations in Climate Models (CLASSIC) aerosol scheme. CLASSIC is the “bulk” (mass-based) aerosol scheme used in Hadley Centre Global Environment Model version 2 (HadGEM2), including Hadley Centre contributions to the fifth Coupled Model Intercomparison Project (CMIP5: Bellouin *et al.*, 2011). CLASSIC includes a range of aerosol species (sulphate, soot, organic carbon from fossil fuel and biofuel, biomass-burning aerosol, sea salt, and mineral dust) as separate externally mixed species with specified physical and optical properties. The soot species takes emissions from fossil-fuel and biofuel emissions of black carbon (BC). A full description of the scheme is available in the appendix of Bellouin *et al.* (2011), and more detail on the simplified version is given in Appendix.

The campaign also made use of global and regional model forecasts from NCMRWF. The NCMRWF global model uses the GA6.1/GL6.1 configuration, following the MetUM operational model. Further details of the implementation and data assimilation of the NCMRWF global Unified Model (NCUM) are given in Rakhi *et al.* (2016) and George *et al.* (2016b), respectively. Regional model configurations of NCUM are based on the tropical version of the MetUM

with 4.0- and 1.5-km horizontal grid length resolution over the Indian domain. Lateral boundaries are supplied from the operational NCMRWF global model at 3-hr intervals and are initialized from the same driver model. The models use 80 vertical levels with a top at 38.5 km and 14 model levels below 1 km, where the planetary boundary layer is resolved efficiently. The model time step is 60 s and forecasts are run for a lead time of 75 hr. In a similar manner to the Met Office 4.4-km LAM, the convection in the NCMRWF regional models is explicit, that is, the subgrid-scale deep and midlevel convection is not parametrized. The subgrid turbulence scheme used here is the blended scheme using a mixing factor of 0.5. The model employs 30-m resolution Indian Space Research Organisation (ISRO) land-use land cover (LuLc) over the Indian region, along with NASA Shuttle Radar Topographic Mission (SRTM) 90-m digital elevation map orography. ISRO LuLc gives recent and updated information about the vegetative and nonvegetative model tiles for the India region. Further details of NCMRWF 1.5-km and NCMRWF 4-km configurations, and the benefits they provide for rainfall prediction over India, are given in Jayakumar *et al.* (2017) and Mamgain *et al.* (2018), respectively.

The skill of the global and regional forecasts made using the MetUM models during the 2016 monsoon season will be documented in a future paper (Ashis Mitra, personal communication 30th April 2019). In the medium range, the model has a tendency to establish a ridge pattern over northwest India and a deeper trough in the northern portion of the monsoon trough, seen in the 850-hPa winds. The ridge pattern at 850 hPa is associated with an anticyclonic systematic error over northwest India that has been documented in previous studies using the MetUM (e.g., Johnson *et al.*, 2016; Levine and Martin, 2018; Keane *et al.*, 2019) and is also found in other models (e.g., George *et al.*, 2016a; Srivastava *et al.*, 2017). Although there is enough moisture available over the Indian region, the ridge pattern does not favour convection and, as a result, a dry bias is seen over northwest India and Bay of Bengal regions. Conversely, the stronger monsoon trough creates a positive rainfall bias around the monsoon trough regions of the northern plains.

Seasonal forecasts were made by the operational global seasonal forecasting system GloSea5 (MacLachlan *et al.*, 2015). In the operational system that was in place during 2016, two seasonal forecast ensemble members were initialized every day and integrated for 210 days. Three weeks of ensemble members (a total of 42 members) are combined to create the seasonal forecast. These are bias corrected using a 14-year (1996–2009), three-member hindcast set initialized on the 1, 9, 17, and 25 of each month. A total of 12 ensemble members from the four nearest weeks of hindcasts are weighted, combined, and then used to bias-correct the forecasts. Johnson *et al.* (2017) demonstrated that GloSea5 has similar skill in predicting the Indian summer monsoon to

other state-of-the-art seasonal forecast systems, with higher skill for the large-scale monsoon circulation than for Indian monsoon rainfall.

### 3 | METHODOLOGY

At the Met Office, forecasts were run using the standard operational global analysis-forecast cycle, in which analyses are produced (using a Hybrid Ensemble 4D-Var data assimilation (DA) system described in Rawlins *et al.*, 2007; Clayton *et al.*, 2013) at 0000, 0600, 1200 and 1800 UTC. Seven-day (168-hr) forecasts are run twice a day from the 0000 and 1200 UTC analyses, while three-day (72-hr) forecasts are run from the 0600 UTC and 1800 UTC analyses. Regional configurations at the Met Office were initialized four times a day and run out to T+60. At NCMRWF, global model forecasts are initialized once per day at 0000 UTC and run for 10 days, while the 4- and 1.5-km regional models were initialized once per day at 0000 UTC and run for three days.

The aerosol model was run from the operational global model's initial conditions, with the non-dust aerosol concentrations initialized from zero for the first run, and then from the previous 6-hr forecast, making the non-dust aerosols a free-running/unconstrained component within the data assimilation cycle. Although the new non-dust aerosols were available, the calculation of their radiative impact used the same aerosol climatology as the operational model, firstly because the radiative impact of an experimental aerosol forecast could have been severely detrimental to the quality of the forecast, and secondly to maintain consistency between the aerosol fields and the atmospheric circulation, which was updated using the operational forecast start conditions. The aerosol global model was operated, in research mode, from March 2016 until September 2017. It should be noted that, as a research model without access to operational-level computing resources, the aerosol forecasts would complete and be available for use 6–12 hr later than the operational forecasts.

Forecast imagery was produced from each of the Met Office forecasts, in the form of regional maps from a wide range of meteorological fields, for example, winds, temperature, humidity, cloud properties, precipitation, and aerosol concentrations, as well as cross-sections through a set of prespecified transects (Figure 1). The forecast imagery was produced using the Iris library (MetOffice, 2013), and the ImageMetaTag library (Brooks, 2015) was used to organize and present the images into a user-friendly web display system for the mission scientists, who examined them prior to holding a daily briefing with the air crew and the instrument operators and (by teleconference) with forecasters and researchers from the wider INCOMPASS team (see Turner *et al.*, 2019). Overall, the forecasts were found to be quite consistent between the different model configurations, and the

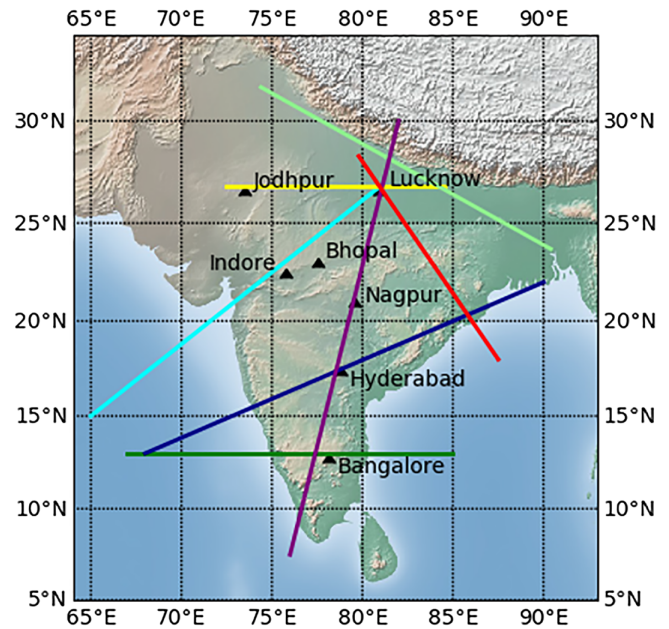


**FIGURE 1** Map of India showing the locations of cross-sections plotted regularly from forecasts for use in the flight campaign

range of outcomes provided a subjective measure of the uncertainty that was useful for flight planning. The kilometre-scale models provided additional local detail that was particularly useful in planning for the monsoon depression flight. These models are also known to represent the timing of the diurnal cycle of rainfall better than lower resolution models (e.g., Willetts *et al.*, 2017b; Mamgain *et al.*, 2018; Stratton *et al.*, 2018) and were therefore particularly useful for planning the southern phase flights to sample different phases of the diurnal cycle.

Seasonal forecasts for June made by GloSea5 were examined during the two months prior to the campaign, in order to assist planning for the first northern phase. During the pre-campaign period, reference was also made to the experimental real-time forecasts made by the Extended Range Prediction group of the Indian Institute of Tropical Meteorology (IITM) using their Ensemble Prediction system (ERPAS)<sup>1</sup> based on the Climate Forecast System Model Version 2 (CFSv2). In addition, the monsoon observations, forecasts, and press releases issued by the India Meteorological Department<sup>2</sup> were monitored.

Since a major aim was to sample both preonset and postonset conditions over northern India, forecasts of monsoon onset (as indicated by thermodynamic and dynamic precursors) from the NCUM 10-day forecasts were also examined. Daily variations of the 850-hPa kinetic energy (KE: Pearce and Mohanthy, 1984; Ramesh *et al.*, 1996), total precipitable water content (TPWC: Ramesh Kumar *et al.*, 2009), and tropospheric (1,000 hPa–100 hPa) temperature gradient (TT)

<sup>1</sup><https://www.tropmet.res.in/erpas/>

<sup>2</sup>[http://www.imd.gov.in/pages/monsoon\\_main.php](http://www.imd.gov.in/pages/monsoon_main.php)

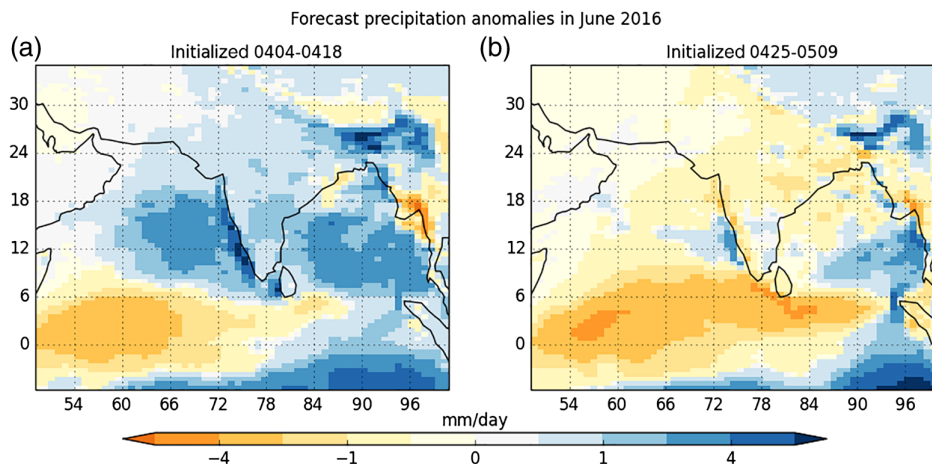


**FIGURE 2** Forecast rainfall anomalies (mm/day) from GloSea5 seasonal forecasts initialized on (a) April 4, 11, and 18, and (b) April 25, and May 1 and 9

index described by Xavier *et al.* (2007) are monitored routinely at NCMRWF from the first week of May. Onset is determined when daily values of 850-hPa KE over the Arabian Sea region  $0^{\circ}\text{N}$ – $19.5^{\circ}\text{N}$ ,  $55.5^{\circ}\text{E}$ – $75^{\circ}\text{E}$  robustly exceed  $60\text{ m}^2/\text{s}^2$ . The KE over the Arabian Sea helps transport the moisture required for precipitation over peninsular India during onset. Thus, total moisture content over peninsular India ( $0^{\circ}\text{N}$ – $15^{\circ}\text{N}$ ,  $70^{\circ}\text{E}$ – $95^{\circ}\text{E}$ ) prior to the onset over Kerala is also a good parameter to monitor the progress of the monsoon over India. Ramesh Kumar *et al.* (2009) showed that the TPWC builds up gradually over the two months prior to monsoon onset, exceeding values of around 52 mm after the beginning of May. This is considered as a necessary condition for monsoon onset in the subjective assessment made by NCMRWF. The TT index measures the difference in vertical mean temperature between 700 and 300 hPa averaged between a northern box ( $10^{\circ}\text{N}$ – $35^{\circ}\text{N}$ ,  $30^{\circ}\text{E}$ – $110^{\circ}\text{E}$ ) and a southern box ( $15^{\circ}\text{N}$ – $10^{\circ}\text{N}$ ,  $30^{\circ}\text{E}$ – $110^{\circ}\text{E}$ ). With the commencement of the Indian summer monsoon, the centre of heat release associated with deep convection moves from the tropical Indian Ocean to the subtropics. The day when the TT index changes from negative to positive is generally close to the onset day of the monsoon. NCMRWF also monitors the dynamical monsoon onset using the criteria defined by Wang *et al.* (2009). Onset is determined to occur when the daily mean zonal wind at 850 hPa averaged over the region  $5^{\circ}\text{N}$ – $15^{\circ}\text{N}$ ,  $40^{\circ}\text{E}$ – $80^{\circ}\text{E}$  exceeds  $6.2\text{ m/s}$ , with the proviso that westerly wind averaged over this region in the ensuing 6 days also exceeds  $6.2\text{ m/s}$ . Although the thresholds chosen for these onset indicators are largely based around their values on June 1 (which is the climatological onset date for monsoon rainfall at Kerala), the thermodynamic and dynamical indicators of onset monitored by NCMRWF measure slightly different aspects of the onset, on a range of spatial scales. Therefore, they would not all be expected to indicate exactly the same onset date. Instead, they are considered together in a subjective assessment before a forecast of early or late onset is issued.

## 4 | SEASONAL OUTLOOK AND ONSET

The Met Office Global Seasonal Forecasting System version 5 (GloSea5) is a coupled initialized global operational seasonal forecasting system (MacLachlan *et al.*, 2015). Previous studies have shown that GloSea5 provides skilful predictions of the large-scale monsoon circulation and modest skill for predicting monsoon rainfall (Johnson *et al.*, 2017; Jain *et al.*, 2018). A recent study (Chevuturi *et al.*, 2018) demonstrated further that, while predictions of the exact date of monsoon onset over India remain elusive, GloSea5 has skill in predicting category-wise monsoon onset, using early, normal, or late tercile categories.

Forecasts from GloSea5 initialized on three start dates in early April indicated that June rainfall totals over India were likely to be slightly above normal (Figure 2a). This was in response to cooling sea-surface temperatures in the eastern Pacific during the spring as the previous winter's El Niño decayed (see Rao *et al.*, 2017). However, the development of a convectively active phase of the Madden–Julian Oscillation (MJO) over the Indian Ocean during May was associated with the development of a monsoon depression over the southwest Bay of Bengal that resulted in the advance of the monsoon into parts of the southern Bay of Bengal, Nicobar Islands, and adjoining Andaman Sea two days ahead of its normal date (Rao *et al.*, 2017). While this deep depression, which developed into a cyclonic storm, provided heavy rainfall over the east coast of the Indian peninsula from mid-May, the cross-equatorial flow remained weak and largely zonal, preventing moisture transport into the Arabian Sea. Forecasts from GloSea5 initialized on three start dates in late April/early May (Figure 2b) were influenced by the developing MJO conditions and predicted a delayed onset and a rather drier than normal June. These contrasting forecasts illustrate that such subseasonal variability is often unpredictable on seasonal

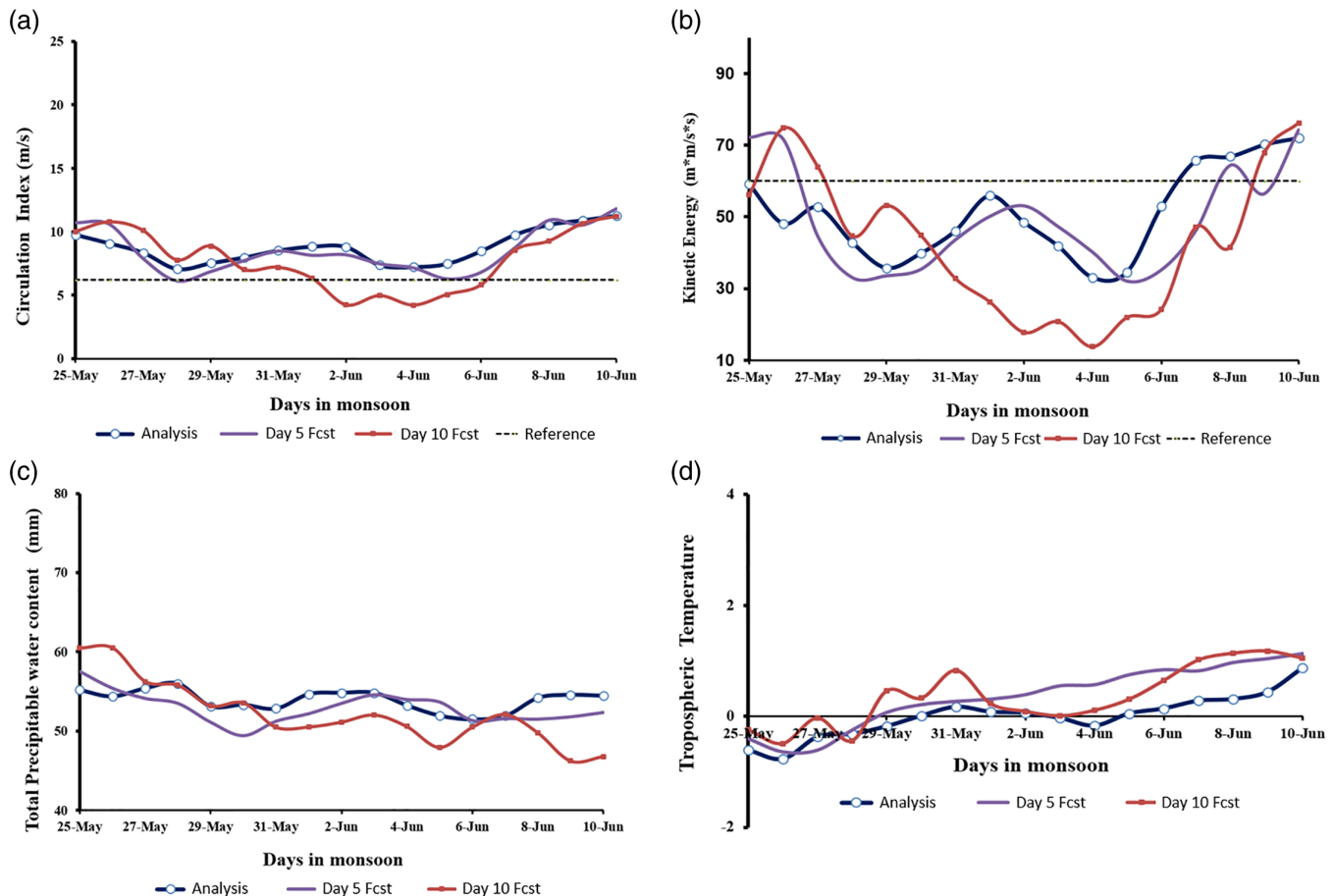


**FIGURE 3** Monsoon onset indicators as forecast by the NCUM between May 27 and June 10. Five-day (purple) and 10-day (red) forecasts, valid on the days indicated, are shown, along with the equivalents from the model analyses (blue line with dots). (a) Dynamical index defined by Wang *et al.* (2009); (b) KE indicator defined by Pearce and Mohanthy (1984); (c) TPWC indicator defined by Ramesh Kumar *et al.* (2009); (d) TT index defined by Xavier *et al.* (2007)

time-scales, so that the developing MJO, and its influence on the monsoon onset, was not represented in the forecasts initialized at the start of April. Rao *et al.* (2017) showed that, during June 2016, rainfall activity over India as a whole was below normal, with only a few areas of the southern peninsula receiving excess rainfall.

On May 15, 2016, the India Meteorological Department issued a Press Release stating their statistical model prediction that the onset at Kerala would be delayed until June 7,<sup>3</sup> around one week later than its usual date of June 1. The ERPAS forecast issued by IITM on May 16, 2016 suggested that, while a synoptic-scale vortex was likely to form over the Arabian Sea and travel northwards along the west coast during the last week of May, generating rainfall along the west coast, rainfall over the southern parts of peninsular India was likely to be below normal during the first week of June. Although there was some variation between the forecast onset dates from the various monsoon onset indicators by the NCUM (Figure 3), overall the forecasts with 5-day lead time (and

even those with 10-day lead time) also suggested that onset at Kerala would be delayed by around one week. The forecasts were accurate; onset at Kerala occurred on June 7 (one week later than climatology). This was favourable for the field campaign, which, although due to begin in late May, was delayed through bureaucracy until June 11. Subsequently, a slow northward progression meant that monsoon rains did not arrive in the northern campaign base at Lucknow until after June 20, by which time the campaign base had moved to its southern location.

The second northern phase of the campaign started on June 28. By this time, according to reports from the India Meteorological Department, the monsoon had progressed northwards into the southeastern part of the region of interest, thereby offering the opportunity to sample the Indo-Gangetic Plain (IGP) in postonset conditions. Forecasts of the rainfall for the second northern phase were examined daily from June 24 onwards. The timing of onset in northern India was influenced by the passage of a monsoon depression northwards through the Bay of Bengal during the last two weeks of June and its subsequent landfall into central India in early July (Rao *et al.*,

<sup>3</sup>[https://www.tropmet.res.in/~kolli/MOL/Monsoon/year2016/for\\_MOK.pdf](https://www.tropmet.res.in/~kolli/MOL/Monsoon/year2016/for_MOK.pdf)

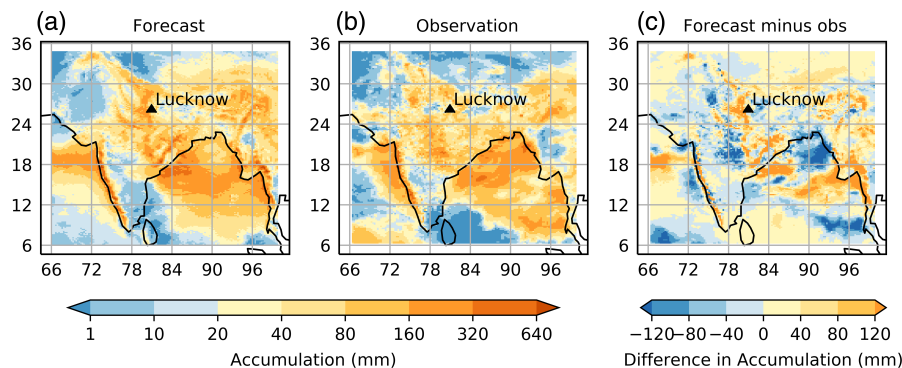


**FIGURE 4** Accumulated rainfall (mm) between June 28 and July 3, 2016 in (a) the 10-day forecast from the global NCUM initialized on June 24, (b) observations from the merged Global Precipitation Measurement (GPM) satellite and gauge product (Mitra *et al.*, 2009), and (c) forecast minus observation difference

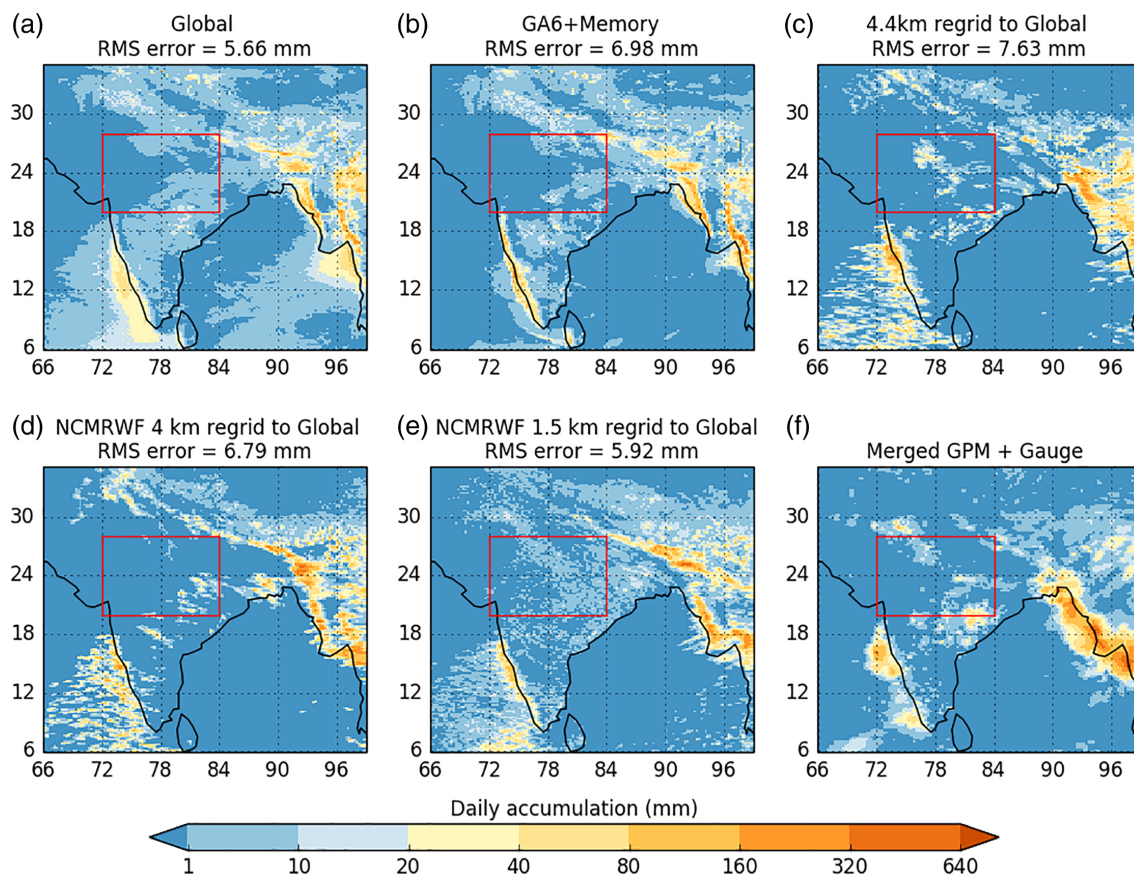


**FIGURE 5** (a)–(e) Forecast and (f) observed accumulated rainfall (mm) on June 11, 2016, from different model configurations (all regridded to the 17-km global model grid) initialized at 1200 UTC on June 9. RMS errors compared with the observations over the red box are provided in the panel titles

2017). This synoptic event was well forecast (see section 5.3), and the predicted rainfall accumulation between June 28 and July 3 from the 10-day forecast initialized on June 24 verified well with observations (see Figure 4), with the exception of a lack of rainfall in the head of the Bay of Bengal and over central India. Such consistency permitted useful planning for the transit flight between the southern and northern bases (see Turner *et al.*, 2019), and for the first flights of the second

northern phase to be carried out while the team was still based in Bengaluru.

## 5 | CASE STUDIES

### 5.1 | Aerosols in the IGP region

The first flight of the campaign took place on June 11, 2016, with the intention of sampling preonset conditions across the

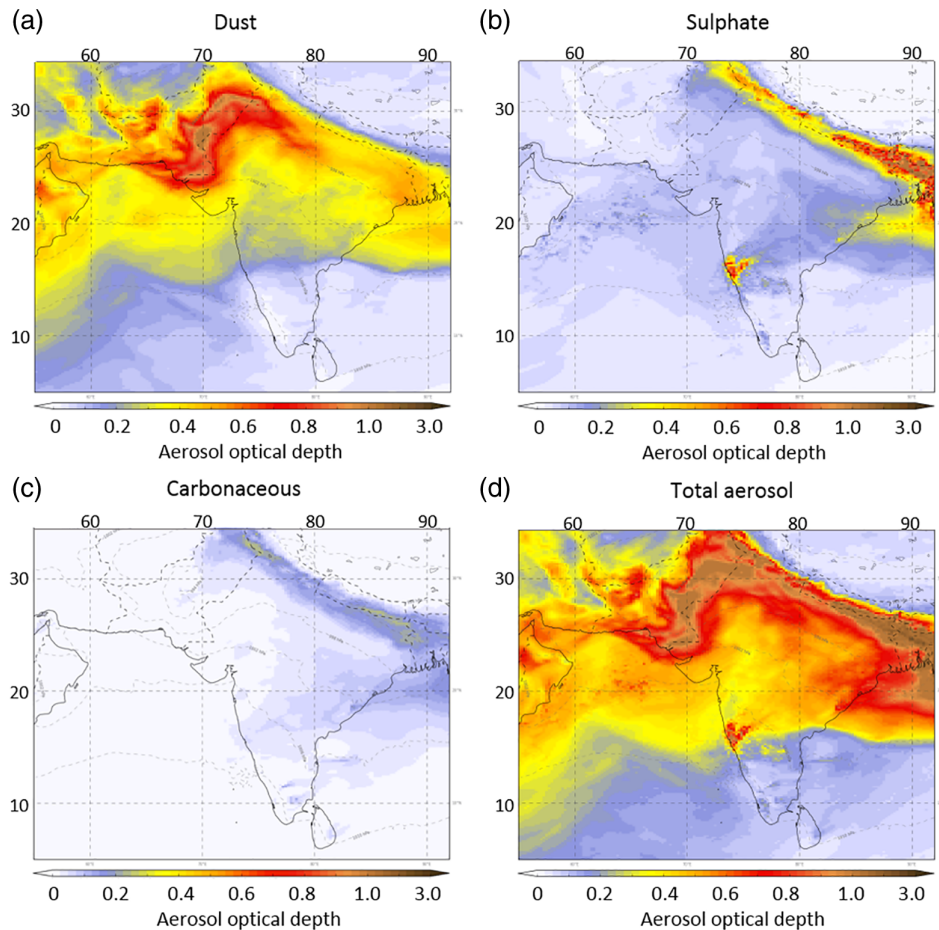


**FIGURE 6** Aerosol optical depth forecasts from the research aerosol model of (a) mineral dust, (b) sulphate, (c) carbonaceous, and (d) total aerosol, for 0600 UTC on June 11, 2016, by the global model initialized at 1800 UTC on June 8

IGP. Rainfall forecasts for June 11 (Figure 5), initialized on June 9, indicated consistently that conditions over the region on June 11 would be mostly dry, while the aerosol forecasts initialized on June 8 from the global configuration with the simplified CLASSIC aerosol scheme included (the aerosol model output was available later than that from the operational model) suggested that significant aerosol optical depths ( $AOD > 0.5$ ) would be found over a large area of the IGP (Figure 6). The aerosol forecasts suggested this would be primarily mineral dust, from a dust event occurring in Pakistan, but it would include  $AOD > 0.1$  for both industrial sulphate and carbonaceous aerosols.

In addition to the maps, forecast cross-sections of total dust concentration and wet-bulb potential temperature ( $\theta_w$ ) passing through Jodhpur, Jaipur, and Lucknow, shown in Figure 7a,c, indicated that a layer of dust and other aerosol was trapped beneath a layer of dry air between 3 and 8 km altitude. Such elevated aerosol layers are common in the IGP region during the premonsoon and have been shown to originate over the desert regions to the northwest (Das *et al.*, 2013; Brooks *et al.*, 2019). Aerosol concentrations were forecast to be greatest to the west of Lucknow, with their maxima over the Great Indian Desert. On the basis of these forecasts, a

flight was planned northwestwards from Lucknow across the IGP towards New Delhi and turning southwestwards towards Jaipur in semi-arid northwest India. Stacked straight and level runs were planned through a deep aerosol layer to examine the impacts of aerosol on downwelling shortwave fluxes for comparison with models, and to sample the aerosol particles in situ. Therefore, accurate forecasting of the location, height, and depth of the aerosol layer across the region was essential for flight planning.

Figure 7b,d shows the model analysis cross-sections of dust concentration and  $\theta_w$  at 0600 UTC (11:30 local time) on June 11. These confirm the accuracy of the forecasts on which the flight plans were based. The observations made during this flight, combined with those from the other flights over northern India sampling premonsoon and postonset conditions, are described in detail in Brooks *et al.* (2019). Their analysis of the aerosols observed in this flight shows that the aerosols were detected broadly as had been forecast, although the forecast aerosol layer was overly smoothed out in the vertical in the model compared with the observations. Brooks *et al.* (2019) concluded that the data collected during these flights will fill significant gaps in previous understanding of aerosols in the IGP region, due to their temporal and spatial

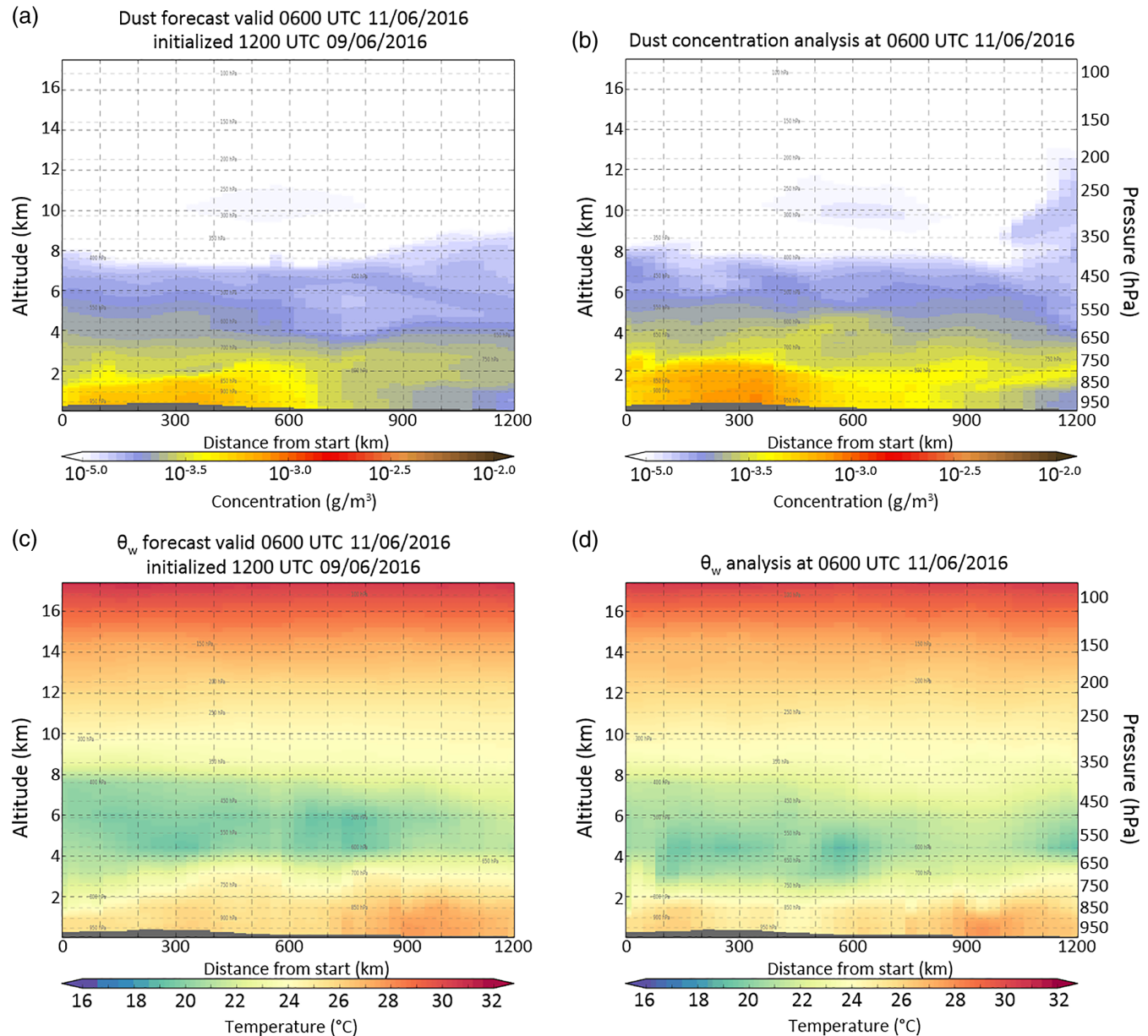


**FIGURE 7** Forecast cross-sections, between  $72.5^{\circ}\text{E}$  and  $84.5^{\circ}\text{E}$ , at  $26.8^{\circ}\text{N}$ , of (a) dust concentration ( $\text{g/m}^3$ ) and (c) wet-bulb potential temperature ( $\theta_w$ ,  $^{\circ}\text{C}$ ) for 0600 UTC on June 11, 2016 by the global model initialized at 1200 UTC on June 9. Panels (b) and (d) show global model analyses of dust concentration and  $\theta_w$  at 0600 UTC on June 11

coverage, to which the availability of accurate forecasting for flight planning clearly contributed.

## 5.2 | Regime change over southern India

The southern phase of the field campaign took place between June 21 and 28, 2016. The FAAM aircraft was based in Bengaluru and flew missions to the east and to the west, sampling the spatial and temporal variations over ocean and land, including land/sea contrasts, orographic enhancement, rain shadow, diurnal cycle, and the effects of the Boreal Summer Intraseasonal Oscillation (BSISO). The dynamic and thermodynamic structure of the monsoon during this phase of the

campaign is documented in detail by Fletcher *et al.* (2019) who showed that, during this period, the rainfall regime to the west of Bengaluru underwent a transition from offshore to coastal rainfall between June 21–24 and June 25–28, which was related to the passage of an active phase of the BSISO. The diurnal cycle of both regimes was sampled by repeating flights over the same path at different times of day.

Figure 8a shows the seven-day forecast time evolution of rainfall across the Indian peninsula from  $12^{\circ}\text{N}$ – $14^{\circ}\text{N}$  during the southern phase of the campaign, initialized at 1200 UTC on June 20, 2016. This can be compared directly with the observed time evolution of rainfall shown in Fletcher *et al.* (2019), their fig. 5 (also included as Figure S1). The initial

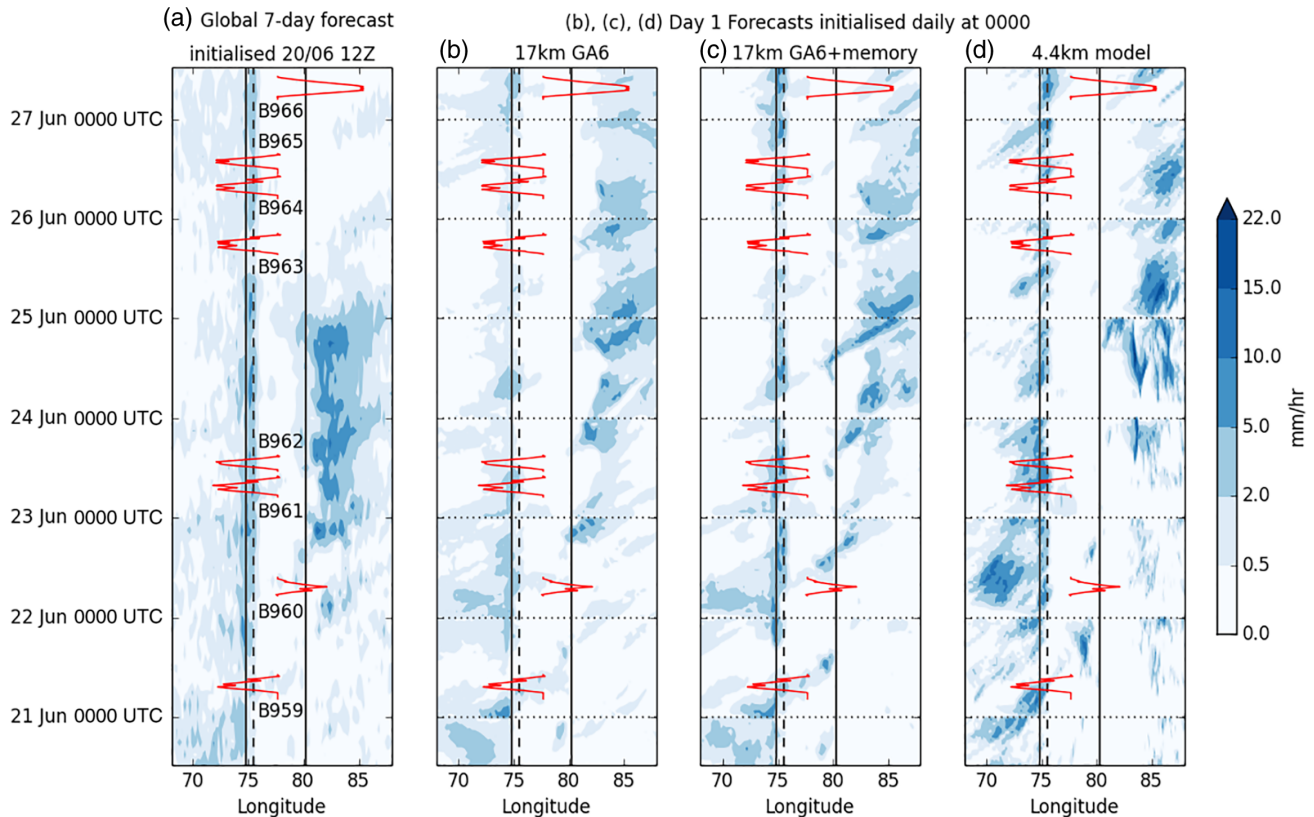


**FIGURE 8** Hovmöller of diagram 3-hr rainfall (mm/hr) averaged over  $12^{\circ}\text{N}$ – $14^{\circ}\text{N}$ , from (a) a seven-day forecast by the global model initialized at 1200 UTC on June 20, 2016, and (b–d) day 1 forecasts initialized daily at 0000 UTC in the (b) global GA6, (c) GA6+memory, and (d) 4.4-km configurations. Flight paths are overlaid in red. Note the nonlinear colour bar. Solid black lines indicate the coasts; a dashed line indicates the peak of the Western Ghats. Dotted lines indicate the initialization time of each 1-day forecast

seven-day forecast was reasonably successful in capturing the offshore and coastal phases of the rainfall regime, although the transition between the two occurred a little earlier in this forecast than in reality. The passage of a monsoon low-pressure system through the Bay of Bengal (see next section) was also forecast successfully at three days lead time. This evolution in the spatial rainfall pattern was associated with the northward movement of a southeast-to-northwest oriented band of rainfall over the Arabian Sea and Bay of Bengal; this band itself was associated with the active phase of the BSISO.

Planning for these flights involved consideration of the location of the main areas of rainfall during daytime and night-time. The seven-day forecast represented the diurnal pattern in rainfall well over the Arabian Sea during the offshore phase (compare Figure 8a with Figure S1), with the heaviest rainfall occurring in the morning (0000 UTC is 5:30 a.m. local time) and the least rain falling in the evening. During the coastal phase, the forecast rainfall was maximum at around 0900 UTC (14:30 local), somewhat earlier than observed (and characteristic of the diurnal cycle of convection over land in models: Stirling and Stratton, 2012).

In addition, the coastal phase was accompanied by an intrusion of dry air from the northeast at midlevels, which

suppressed deep convection and rainfall over the Arabian Sea and allowed moisture to accumulate at lower levels. Forecasting the time and height at which this dry intrusion would be found was essential in order to ensure that this vertical contrast and its development would be captured during the flights. Figure 9a,c shows the forecast cross-sections of wet-bulb potential temperature, initialized on June 21, 2016 at 1200 UTC and valid on June 22 (T+24) and 26 (T+120), which were used for flight planning at the start of the southern phase. These indicated the presence of a dry-air intrusion between 2 and 6 km altitude (800–500 hPa) encroaching the peninsula over the period of the forecast and trapping increasingly moist air in the boundary layer. Global model analyses from these two days (Figure 9b,d) verified that this regime change was forecast sufficiently well for the planned flights to sample the thermodynamics structure with little alteration.

On the basis of the seven-day forecast examined on June 20, six flights heading westwards from Bengaluru to sample the contrasts in rainfall across the Western Ghats were planned, along with two flights eastward into the Bay of Bengal. Flights B962 and B965 were evening flights (take-off at 11:30 UTC, 17:00 local), while B963 was at night (take-off at 1600 UTC, 21:30 local). The other panels in Figure 8 show

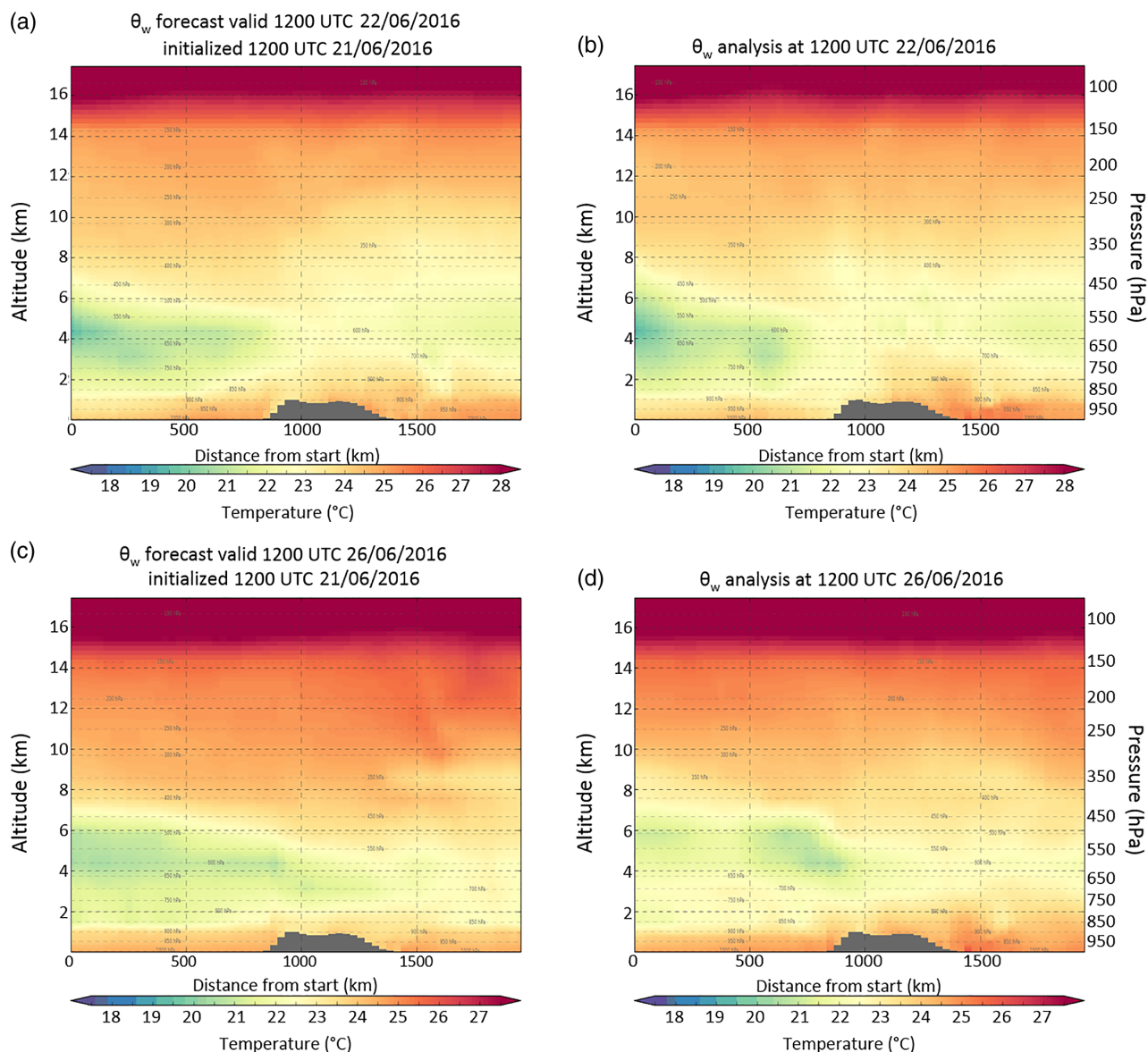


**FIGURE 9** (a,c) Global model forecasts initialized on June 21, 2016, and (b,d) analyses of wet-bulb potential temperature ( $\theta_w$ , °C): cross-sections at 13°N between 67°E and 85°E. Valid for (a,c) June 22 at 1200 UTC and (b,d) June 26 at 1200 UTC, as used during the field campaign to plan the southern phase flights

day-1 forecasts initialized daily at 0000 UTC from the global operational model and from the other model configurations. These illustrate how the forecasts were updated through the period, allowing more detailed planning to be carried out on a daily basis. At shorter lead times, the forecasts captured more of the offshore rainfall and the contrast between the two phases, particularly in the 4.4-km configuration. This is illustrated in Figure 10, which shows the mean rainfall between 12°N and 14°N during the two phases from the various forecasts. The timing of the diurnal cycle of the rainfall, particularly the occurrence of evening rainfall, was captured in the daily forecasts with the 4.4-km model and in the research configuration with convective memory (Figure 8c,d). These configurations were therefore particularly useful for planning the evening and night-time flights.

As discussed in Fletcher *et al.* (2019), these forecasts allowed plans to be made to sample the differing conditions in six flights to the west of Bengaluru, over more or less the same flight path, between June 21 and 26, 2016. Since INCOMPASS was not permitted to drop sondes during flights, the flight plans needed to include multiple flight-track profiles and level runs at different heights based on the forecasts in order to sample the atmospheric conditions adequately. Although continual monitoring of the forecasts on a daily basis allowed flight plans to be refined over this period, the quality of the initial seven-day forecast was sufficient for much of this planning to be carried out in advance. As a result, Fletcher *et al.* (2019) were able to characterize the regime change between the offshore and coastal phases during this period using aircraft, radiosonde, and ground-based

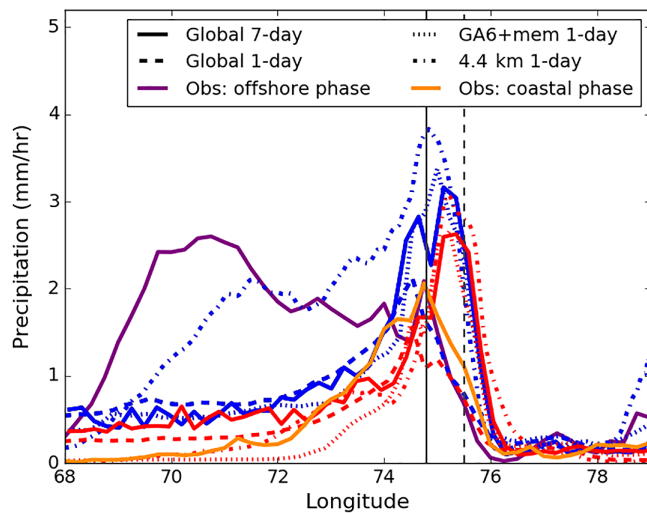


**FIGURE 10** Longitudinal cross-sections of 3-hr rainfall (mm/hr) averaged over 12°N–14°N, from a seven-day forecast by the global model initialized at 1200 UTC on June 20, 2016 (solid lines), and day 1 forecasts initialized daily at 0000 UTC in the global GA6 (dashed), GA6+memory (dotted), and 4.4-km (dot-dashed) configurations. Colours indicate the time periods of the offshore (blue: 0300 UTC on June 21 to 0300 UTC on June 24) and coastal (red: 0300 UTC on June 25 to 0300 UTC on June 28) phases as identified by Fletcher *et al.* (2019). Observations from the merged GPM satellite and gauge product (Mitra *et al.*, 2009) for the two phases are shown in purple (offshore) and orange (coastal)

data. They concluded that the observations would provide a useful framework for detailed climatological studies and modelling experiments, which could be used to test hypotheses with greater rigour.

### 5.3 | Monsoon depression

During the southern phase, it was noted that a low-pressure system was forming in the southern Bay of Bengal. Its potential to develop into a monsoon depression was hinted at in forecasts initialized on June 18, and Figure 11 shows that some characteristics of the observed track were captured in global model forecasts even at 18 days before the flight to sample the depression took place on July 7. Several previous studies have assessed the ability of the MetUM to simulate monsoon depressions (MDs): Hunt and Turner (2017) showed that, in the global operational forecast configuration, forecasts initialized on the same day as the MD had developed a mean track error of 300 km seven days later, and tended to overestimate the system intensity slightly. Levine and Martin (2018), building on work by Karmacharya *et al.* (2016), showed that a regional climate model configuration produced satisfactory monsoon low-pressure system statistics, though their penetration into the peninsula was underestimated, and the results were sensitive to the boundary conditions. Mammagani *et al.* (2018) inspected a depression case study with both global and regional configurations of the NCMRWF version

of the MetUM, finding that associated forecast precipitation had a positive, northward bias.

The forecast location of the depression and associated convective activity on the planned flight day was crucial in order to plan a flight path that would sample its main features. Initial flight planning began a few days before the flight. Forecasts initialized on July 5 from the different configurations (see Figure 12) provided a reasonably consistent location for the low mean sea-level pressure minimum of the depression at around 83°E, 24°N on July 7, with the associated daily accumulated rainfall maximum slightly to the west around 80°E, 24°N in the region of Jabalpur. This was reasonably consistent with the actual analysis from July 7 (Figure 12f), although the forecasts tended to overdeepen the depression and move it further inland than actually occurred. However, the forecast location of the system was sufficiently accurate that the initial estimates for the flight track were not altered much subsequently.

Due to the unprecedented nature of this flight for the FAAM, the flight plan was developed over the course of two days, with close attention to the forecasts. Figure 13c,d shows the complexity of the thermodynamic structure in the 24-hr forecast charts from the 4.4-km regional configuration that were used during flight planning. One aim of the flight was to capture the strong northwesterly inflow to the region of deep organized convection (Figure 13a,b) and to measure the contrasting thermodynamic states of the system. The inflow was characterized by a plume or filament of air with high wet-bulb potential temperature advecting into the core of the depression at 500 hPa in the forecast (Figure 13c). Forecast cross-sections of  $\theta_w$  and relative humidity between the central Arabian Sea and Lucknow (Figure 14) indicated a dry layer between 4 and 6 km altitude, extending from the southwest to the edge of the depression. Therefore, one aim was to transit out of the moist depression core into this dry air at the southwest limit of the upper, outward leg (see planned flight track in Figure 13c). Another aim was to capture something of the surface fluxes (or at least, validate the boundary-layer structure) in the high wind zone to the southwest of the depression.

Particularly crucial to flight planning was the need to avoid deep convection by flying just upwind of it, to the northwest, for safety reasons and in order to sample the moist flow feeding into the rainfall region. The convection-permitting forecasts shown in Figure 12c–e very clearly influenced the flight planning here, although, in the event, the convection was quite different and the aircraft had to fly through the main area of rainfall, making several minor changes in track to thread a path through the most intense convective cores. However, the flight did not deviate more than a few miles from the original planned track.

Figure 14 shows that the forecast thermodynamic structure agreed well with the analyses on July 7, with the analysed position (and moisture content) of the moist air associated

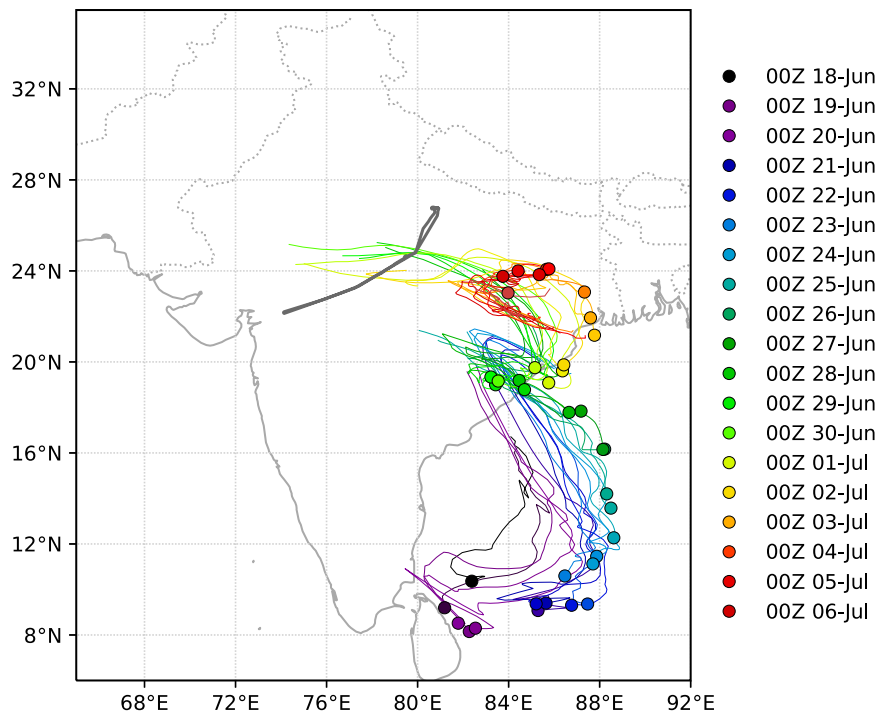


**FIGURE 11** Analysed (dots) and forecast (lines) locations of the monsoon depression, identified using the method of Hunt *et al.* (2016) and Hunt *et al.* (2018), in seven-day global model forecasts initialized at 0000 UTC and 1200 UTC. The thick grey line denotes the path of flight B974 on July 7

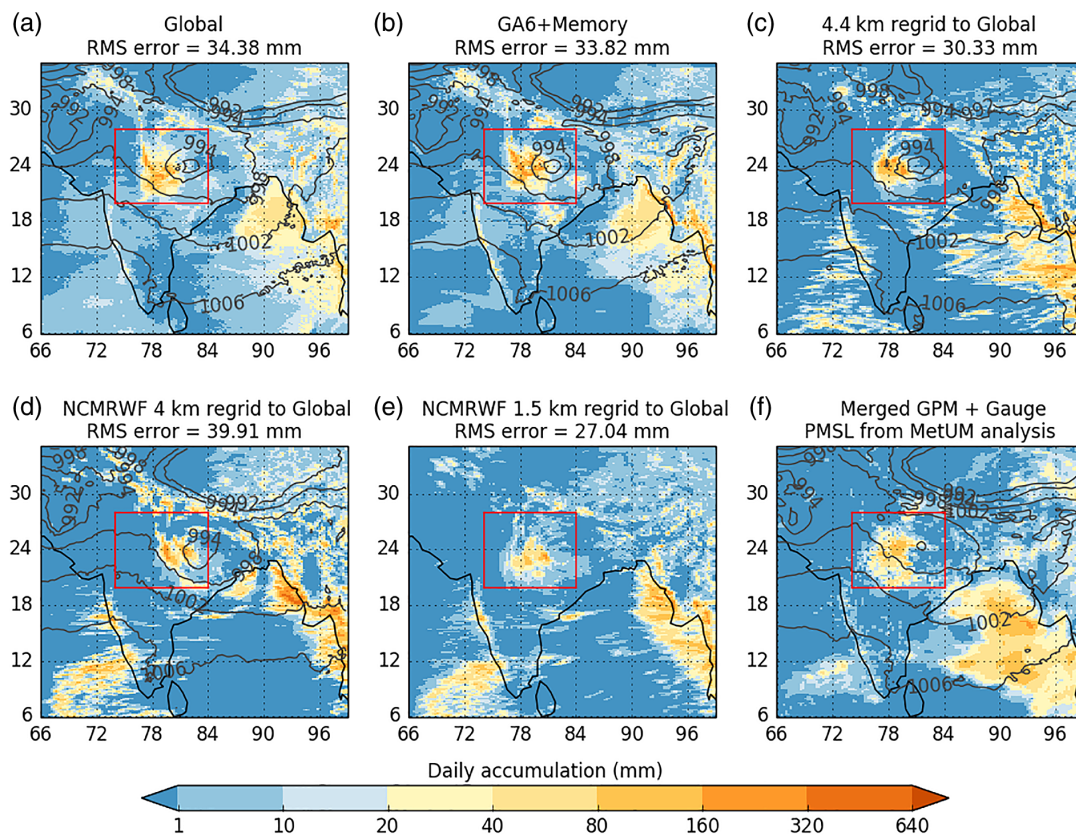


**FIGURE 12** (a)–(e) Forecasts (initialized on July 5) and (f) analysis of daily accumulated rainfall (shaded) and pressure at mean sea level (PMSL) at 0000 UTC (contours) on July 7, 2016, used to plan monsoon depression flight B974. Note that PMSL was not output from the 1.5-km regional configuration. For quantitative comparison, the fields from the 4.4-, 4-, and 1.5-km regional configurations, and from the observations, have been regridded to the global model resolution. RMS errors in rainfall against the observed daily accumulation calculated over the red box are shown in the panel titles

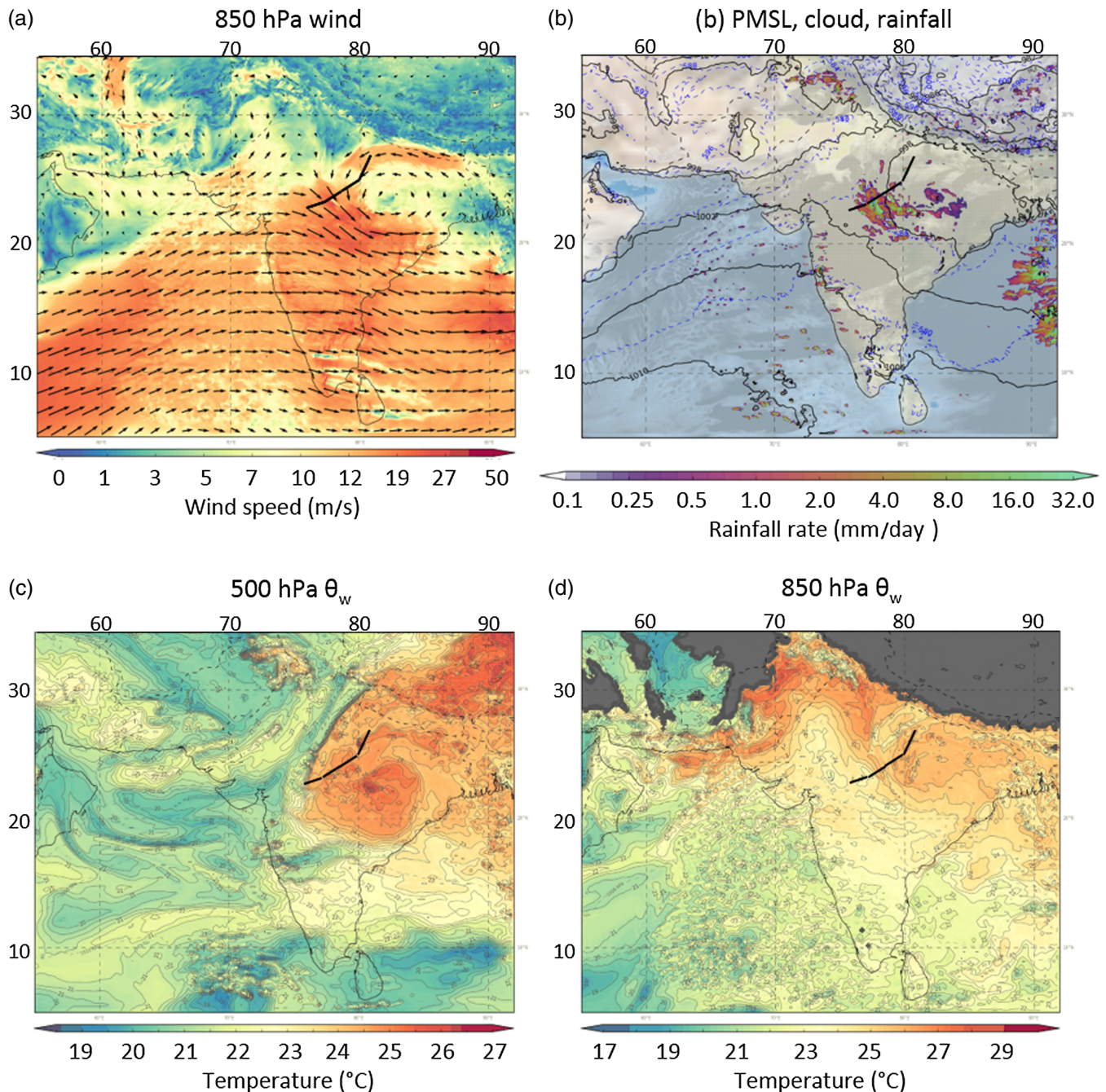


**FIGURE 13** 24-hr forecasts of weather conditions on July 7 from the 4.4-km regional configuration, initialized on July 6 at 0600 UTC, as used in the flight planning for the monsoon depression flight. The planned flight track is superimposed on each panel

with the depression being only slightly to the northeast of (and less than) that in the forecast. Figure 15 shows the flight path superimposed on the analysed fields at 0600 UTC (11:30 local) on July 7. The flight path passed close to the region of lowest pressure and maximum rainfall, as well as the region of maximum 850-hPa winds. Significant cumulonimbus was observed to the north and west of the route, but beyond Bhopal (23°N, 77°E) the convection diminished, and finally, just beyond Indore (22.5°N, 75.5°E), the flight crossed into the dry intrusion from the northwest. This was

a significant air-mass change, occurring over only a few km, also associated with changes in atmospheric composition.

Returning at lower levels between Indore and Bhopal, strong northwesterly winds (around 15 m/s) were observed, representing the strong jet-like flow on the southwestern flank of the depression. Significant increases in equivalent potential temperature were observed as the flight returned into the heart of the monsoon depression, with associated veering of the winds to northerly. Around Bhopal, the maximum rain zone of the system was encountered. The land surface was clearly saturated, with many fields waterlogged and the rivers

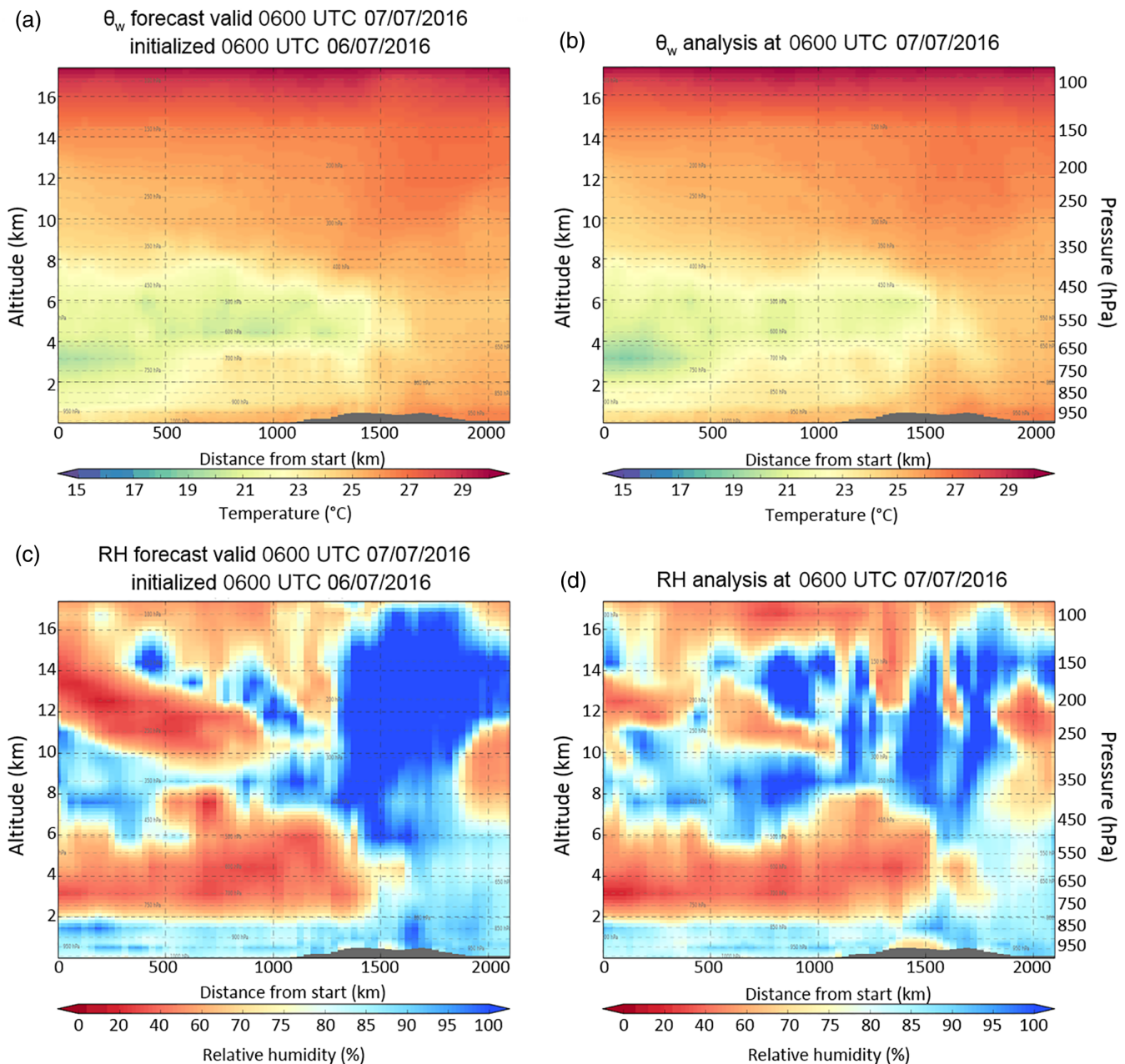


**FIGURE 14** (a,c) Global model forecasts initialized on July 6, 2016 at 0600 UTC, and (b,d) analyses, both valid at 0600 UTC on July 7, 2016: cross-sections of (a,b) wet-bulb potential temperature ( $\theta_w$ , °C) and (c,d) relative humidity (%), between the central Arabian Sea (15°N, 65°E) and Lucknow (26.76°N, 80.88°E) (light blue line in Figure 1), as used in the flight planning for the monsoon depression flight

very high. On emerging from the main area of rainfall to the northeast of Khajuraho (24.5°N, 80°E), the skies cleared to developing congestus and cumulonimbus clouds.

This flight was highly successful and provided a wealth of observations that will be analysed and described in detail in a future article. Mission Scientist, Doug Parker, commented that “these forecasts were critical in defining the flight plan: we wanted to capture the structure of these strong thermodynamic gradients and the shear zone (somewhat reminiscent of a midlatitude warm front?)”.

## 6 | SUMMARY

We have demonstrated how access to multiple forecast products from a variety of configurations at a range of resolutions contributed to successful flight planning for the INCOMPASS field campaign in India in 2016. Accurate forecasting of the monsoon circulation and thermodynamic structure on a particular flying day was crucial for planning flight patterns. In addition, the requirement to file flight plans at least two days in advance, with little scope for major alteration

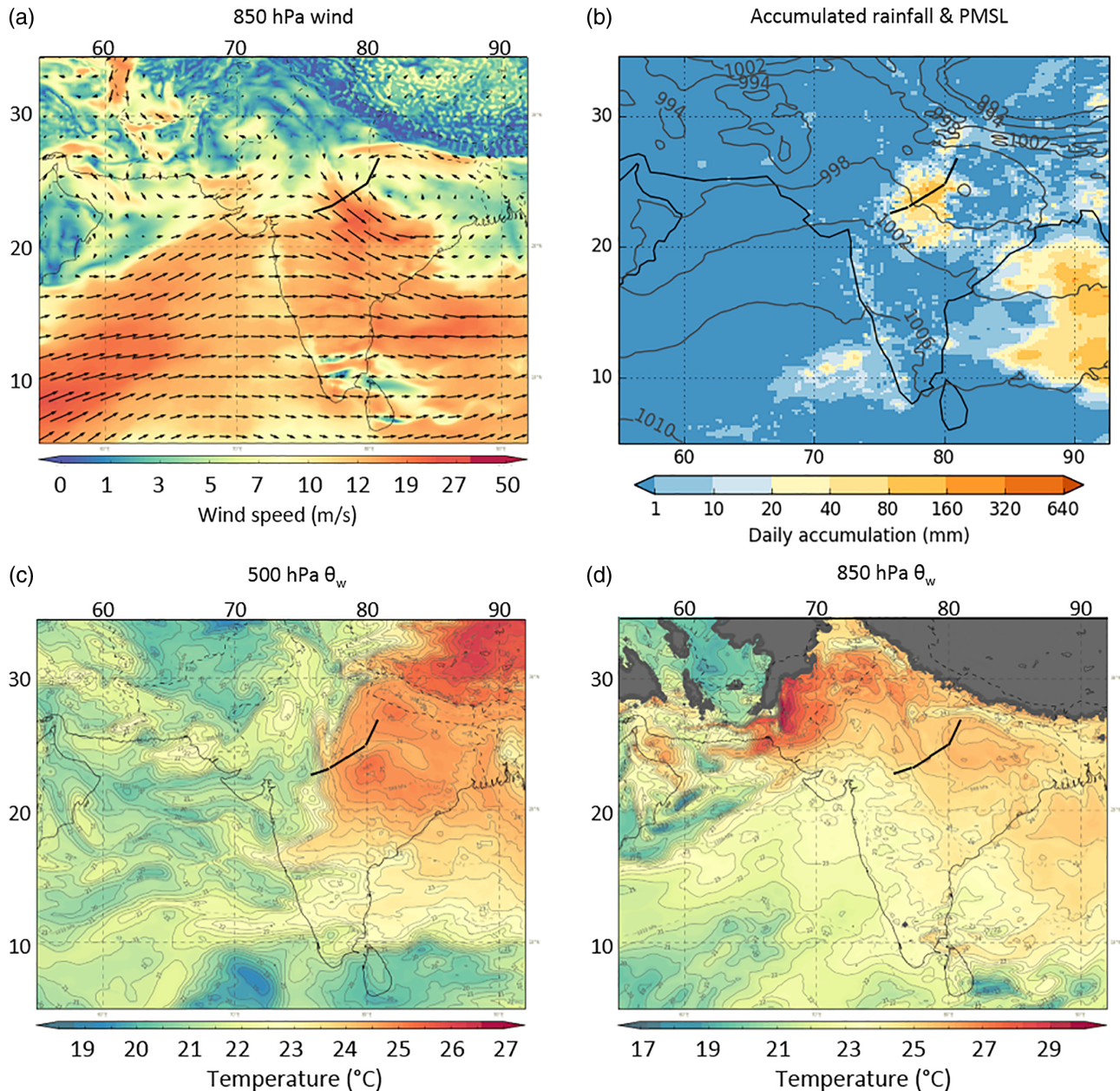


**FIGURE 15** Analysis at 0600 UTC (11:30 local) on July 7, 2016 of (a) winds at 850 hPa, (c,d)  $\theta_w$  at 500 and 850 hPa, respectively, and (b) PMSL and observed accumulated rainfall (as in Figure 12f), with the planned flight track overlaid in solid black lines

thereafter, made the necessity for accurate weather forecasts even greater.

Despite inherent difficulties in forecasting the precise location of deep convective rainfall one or more days in advance, the availability of forecasts from model configurations at various resolutions, with different representations of convection, provided a range of portrayals of the rainfall pattern to the mission scientists. Regional convection-permitting models have known issues (e.g., Lean *et al.*, 2008; Baldauf *et al.*, 2011), but have been shown to provide benefits to forecasting of small-scale structures, at least in the extratropics (e.g., Weusthoff *et al.*, 2010; Fosser *et al.*, 2015), and also provide better timing of the maximum rainfall in the diurnal cycle

over land (Willettts *et al.*, 2017b). The examples provided in section 5 confirm the view reached among the INCOMPASS science team that, between them, the various forecast products captured the main characteristics of the rainfall events sufficiently well that the actual flight tracks did not need to deviate far from their initial planned locations.

Finally, an important outcome of this activity came through regular discussions with Indian forecasters before, during, and after the campaign, which have strengthened links between UK and Indian researchers and forecasters and improved our understanding of the Indian monsoon. We now have a large database of targeted model forecast products for the whole of the 2016 monsoon season. These can be used by

researchers for comparisons with in situ observations as well as for future modelling studies.

## 7 | LEGACY OF FORECASTING ACTIVITY

The forecast data from this campaign are archived and curated at the Met Office and can be made available to researchers. Since the INCOMPASS flight campaign, the ability to provide near-real-time forecasts for observing campaigns has been developed further, and the facility is routinely made available to researchers in the UK and the global community. Since 2016, developments at the Met Office include the creation of a coupled NWP forecasting system, which is currently under trial. In addition, new configurations have been released (Global Atmosphere 7.01/7.1: Walters *et al.*, 2019), which include significant changes to the representation of warm-rain microphysics, the radiative effects of convective cores, heating due to gravity-wave dissipation, and major changes to the convection parametrization, including its closure assumptions. Furthermore, new diagnostics have been included, which allow tracking through the forecast of contributions to changes in potential vorticity (PV) from different parts of the model physics. Such a PV-tracer scheme has been employed by several studies of midlatitude model error (e.g., Chagnon *et al.*, 2013; Gray, 2006). Future work will include making hindcasts of various cases from the field campaign in order to provide more insight into monsoon processes.

## DATA AVAILABILITY STATEMENT

Forecast data relating to the flight campaign are archived and curated at the Met Office and at NCMRWF and are available to researchers upon application.

## ACKNOWLEDGEMENTS

G.M.M. was supported by the Met Office Hadley Centre Climate Programme funded by BEIS and Defra. S.F.M., M.E.B., and S.W. were supported by the Natural Environment Research Council grant NW/L01386X/1 under INCOMPASS. A.K.M., A.J., and D.R. were supported by the India Ministry of Earth Sciences under the National Monsoon Mission. K.M.R.H. was supported by the JPI-Climate and Belmont Forum Climate Predictability and Inter-Regional Linkages Collaborative Research Action via NERC grant NE/P006795/1. Airborne data were obtained using the BAe-146-301 Atmospheric Research Aircraft (ARA) flown by Directflight Ltd. (now Airtask Ltd.) and managed by the Facility for Airborne Atmospheric Measurements (FAAM), which is a joint entity of the Natural Environment Research Council (NERC) and the Met Office. The authors thank

INCOMPASS mission scientist Professor Doug Parker for his insight into the flight planning process for B974. We also thank Margaret Gordon for providing the GloSea5 forecast data.

## CONFLICT OF INTEREST

The authors declare no conflict of interest relating to this work.

## ORCID

Gill M. Martin  <http://orcid.org/0000-0003-0851-6020>

A. Jayakumar  <http://orcid.org/0000-0002-1497-6042>

Kieran M. R. Hunt  <http://orcid.org/0000-0003-1480-3755>

## REFERENCES

- Aiken, A.C., DeCarlo, P.F., Kroll, J.H., Worsnop, D.R., Huffman, J.A., Docherty, K.S., Ulbrich, I.M., Mohr, C., Kimmel, J.R., Sueper, D., Sun, Y., Zhang, Q., Trimborn, A., Northway, M., Ziemann, P.J., Canagaratna, M.R., Onasch, T.B., Alfarra, M.R., Prevot, A.S.H., Dommen, J., Duplissy, J., Metzger, A., Baltensperger, U. and Jimenez, J.L. (2008) O/C and OM/OC ratios of primary, secondary, and ambient organic aerosols with high-resolution time-of-flight aerosol mass spectrometry. *Environmental Science & Technology*, 42, 4478–4485.
- Andres, R.J. and Kasgnoc, A.D. (1998) A time-averaged inventory of subaerial volcanic sulfur emissions. *Journal of Geophysical Research*, 103, 25251–25261.
- Aranami, K., Davies, T. and Wood, N. (2015) A mass restoration scheme for limited-area models with semi-Lagrangian advection. *Quarterly Journal of the Royal Meteorological Society*, 141, 1795–1803.
- Ashis M. Research Scientist-G. (Personal communication, 30th April 2019).
- Baldauf, M., Seifert, A., Förstner, J., Majewski, D., Raschendorfer, M. and Reinhardt, T. (2011) Operational convective-scale numerical weather prediction with the COSMO model: description and sensitivities. *Monthly Weather Review*, 139, 3887–3905.
- Bellouin, N., Rae, J., Jones, A., Johnson, C., Haywood, J. and Boucher, O. (2011) Aerosol forcing in the climate model intercomparison project (CMIP5) simulations by HadGEM2-ES and the role of ammonium nitrate. *Journal of Geophysical Research*, 116, D20206. <https://doi.org/10.1029/2011JD016074>.
- Best, M.J., Pryor, M., Clark, D.B., Rooney, G.G., Essery, R.L.H., Ménard, C.B., Edwards, J.M., Hendry, M.A., Porson, A., Gedney, N., Mercado, L.M., Sitch, S., Blyth, E., Boucher, O., Cox, P.M., Grimmond, C.S.B. and Harding, R.J. (2011) The Joint UK Land Environment Simulator (JULES), model description – part 1: energy and water fluxes. *Geoscientific Model Development*, 4, 677–699.
- Bhat, G. and Narasimha, R. (2007) Indian summer monsoon experiments. *Current Science*, 93, 153–164.
- Boutle, I.A., Eyre, J.E.J. and Lock, A.P. (2014) Seamless stratocumulus simulation across the turbulent gray zone. *Monthly Weather Review*, 142, 1655–1668.
- Brooks, J., Allan, J.D., Williams, P.I., Liu, D., Fox, C., Haywood, J., Langridge, J.M., Highwood, E.J., Kompalli, S.K., O’Sullivan, D.,

- Babu, S.S., Satheesh, S.K., Turner, A.G. and Coe, H. (2019) Vertical and horizontal distribution of sub-micron aerosol chemical composition and physical characteristics across northern India, during the premonsoon and monsoon seasons. *Atmospheric Chemistry and Physics*, 19, 5615–5634.
- Brooks, M.E. (2015) *ImageMetaTag: A Python Package for Tagging, Managing and Presenting Very Large Numbers of Images Created by matplotlib Github Repository*. Exeter: Met Office. Available at: <https://github.com/SciTools-incubator/image-meta-tag>.
- Brown, A.R., Beare, R.J., Edwards, J.M., Lock, A.P., Keogh, S.J., Milton, S.F. and Walters, D.N. (2008) Upgrades to the boundary-layer scheme in the Met Office numerical weather prediction model. *Boundary-Layer Meteorology*, 128, 117–132.
- Chagnon, J.M., Gray, S.L. and Methven, J. (2013) Diabatic processes modifying potential vorticity in a North Atlantic cyclone. *Quarterly Journal of the Royal Meteorological Society*, 139, 1270–1282.
- Chevuturi, A., Turner, A.G., Woolnough, S.J., Martin, G.M. and MacLachlan, C. (2018) Indian summer monsoon onset forecast skill in the UK Met Office initialized coupled seasonal forecasting system (GloSea5-GC2). *Climate Dynamics*, 52, 6599–6617.
- Clark, D.B., Mercado, L.M., Sitch, S., Jones, C.D., Gedney, N., Best, M.J., Pryor, M., Rooney, G.G., Essery, R.L.H., Blyth, E., Boucher, O., Harding, R.J., Huntingford, C. and Cox, P.M. (2011) The Joint UK Land Environment Simulator (JULES), model description – part 2: carbon fluxes and vegetation dynamics. *Geoscientific Model Development*, 4, 701–722.
- Clayton, A.M., Lorenc, A.C. and Barker, D.M. (2013) Operational implementation of a hybrid ensemble/4D-Var global data assimilation system at the Met Office. *Quarterly Journal of the Royal Meteorological Society*, 139, 1445–1461.
- Cusack, S., Slingo, A., Edwards, J.M. and Wild, M. (1998) The radiative impact of a simple aerosol climatology on the Hadley Centre atmospheric GCM. *Quarterly Journal of the Royal Meteorological Society*, 124, 2517–2526.
- Das, S., Dey, S., Dash, S. and Basil, G. (2013) Examining mineral dust transport over the Indian subcontinent using the regional climate model, RegCM4.1. *Atmospheric Research*, 134, 64–76. <https://doi.org/10.1016/j.atmosres.2013.07.019>.
- Derwent, R.G., Collins, W.J., Jenkin, M.E., Johnson, C.E. and Stevenson, D.S. (2003) The global distribution of secondary particulate matter in a 3-D Lagrangian chemistry transport model. *Journal of Atmospheric Chemistry*, 44, 57–95.
- Diehl, T., Heil, A., Chin, M., Pan, X., Streets, D., Schultz, M. and Kinne, S. (2012) Anthropogenic, biomass burning, and volcanic emissions of black carbon, organic carbon, and SO<sub>2</sub> from 1980 to 2010 for hindcast model experiments. *Atmospheric Chemistry and Physics Discussions*, 12, 24895–24954. <https://doi.org/10.5194/acpd-12-24895-2012>.
- Fletcher, J.K., Parker, D.J., Turner, A.G., Menon, A., Martin, G.M., Birch, C.E., Mitra, A.K., Govindankutty, M., Hunt, K.M.R., Taylor, C.M., Houze, R.A., Brodzik, S.R., Bhat, G.S. and Marsham, J.H. (2019) The dynamic and thermodynamic structure of the monsoon over southern India: new observations from the INCOMPASS IOP. *Quarterly Journal of the Royal Meteorological Society*, 1–24. <https://doi.org/10.1002/qj.3439>.
- Fosser, G., Khodayar, S. and Berg, P. (2015) Benefit of convection permitting climate model simulations in the representation of convective precipitation. *Climate Dynamics*, 44, 45–60.
- Fritsch, J.M. and Chappell, C.F. (1980) Numerical prediction of convectively driven mesoscale pressure systems. Part I: convective parametrization. *Journal of the Atmospheric Sciences*, 37, 1722–1733.
- George, G., Rao, D.N., Sabeerali, C.T., Srivastava, A. and Rao, S.A. (2016a) Indian summer monsoon prediction and simulation in CFSv2 coupled model. *Atmospheric Science Letters*, 17, 57–64. <https://doi.org/10.1002/asl.599>.
- George, J.P., Indira Rani, S., Jayakumar, A., Mohandas, S., Mallick, S., Lodh, A. and Rajagopal, E.N. (2016b) *NCUM data assimilation system*. Noida: National Centre for medium range weather forecasting (NCMRWF), Ministry of Earth Sciences. Technical Report NMRF/TR/01/2016
- Granier, C., Bessagnet, B., Bond, T., D'Angiola, A., Denier van der Gon, H., Frost, G.J., Heil, A., Kaiser, J.W., Kinne, S., Klimont, Z., Kloster, S., Lamarque, J.-F., Liouss, C., Masui, T., Meleux, F., Mieville, A., Ohara, T., Raut, J.-C., Riahi, K., Schultz, M.G., Smith, S.J., Thompson, A., van Aardenne, J., van der Werf, G.R. and van Vuuren, D.P. (2011) Evolution of anthropogenic and biomass burning emissions of air pollutants at global and regional scales during the 1980–2010 period. *Climatic Change*, 109, 163–190.
- Grant, A.L.M. (2001) Cloud-base fluxes in the cumulus-capped boundary layer. *Quarterly Journal of the Royal Meteorological Society*, 127, 407–421.
- Grant, A.L.M. and Brown, A.R. (1999) A similarity hypothesis for shallow-cumulus transports. *Quarterly Journal of the Royal Meteorological Society*, 125, 1913–1936.
- Gray, S.L. (2006) Mechanisms of midlatitude cross-tropopause transport using a potential vorticity budget approach. *Journal of Geophysical Research*, 111, D17113. <https://doi.org/10.1029/2005JD006259>.
- Gregory, D. and Allen, S. (1991) The effect of convective downdraughts upon NWP and climate simulations. In: *Proceedings of Ninth Conference on Numerical Weather Prediction*. Denver, CO: American Meteorological Society, 122–123.
- Gregory, D. and Rowntree, P.R. (1990) A mass flux convection scheme with representation of cloud ensemble characteristics and stability-dependent closure. *Monthly Weather Review*, 118, 1483–1506.
- Hunt, K.M. and Turner, A.G. (2017) The effect of horizontal resolution on Indian monsoon depressions in the Met Office NWP model. *Quarterly Journal of the Royal Meteorological Society*, 143, 1756–1771.
- Hunt, K.M.R., Turner, A.G., Inness, P.M., Parker, D.E. and Levine, R.C. (2016) On the structure and dynamics of Indian monsoon depressions. *Monthly Weather Review*, 144, 3391–3416.
- Hunt, K.M.R., Turner, A.G. and Shaffrey, L.C. (2018) The evolution, seasonality and impacts of western disturbances. *Quarterly Journal of the Royal Meteorological Society*, 144, 278–290.
- Jain, S., Scaife, A.A. and Mitra, A.K. (2018) Skill of Indian summer monsoon rainfall prediction in multiple seasonal prediction systems. *Climate Dynamics*, 52, 5291–5301. <https://doi.org/10.1007/s00382-018-4449-z>.
- Jayakumar, A., Sethunadh, J., Rakhi, R., Arulalan, T., Mohandas, S., Iyengar, G.R. and Rajagopal, E.N. (2017) Behavior of predicted convective clouds and precipitation in the high-resolution unified model over the Indian summer monsoon region. *Earth and Space Science*, 4, 303–313. <https://doi.org/10.1002/2016EA000242>.
- Johnson, S.J., Levine, R.C., Turner, A.G., Martin, G.M., Woolnough, S.J., Schiemann, R., Mizielski, M.S., Roberts, M.J., Vidale, P.L., Demory, M.-E. and Strachan, J. (2016) The resolution sensitivity of the South Asian monsoon and Indo-Pacific in a global 0.35° AGCM.

- Climate Dynamics*, 46, 807–831. <https://doi.org/10.1007/s00382-015-2614-1>.
- Johnson, S.J., Turner, A., Woolnough, S., Martin, G. and MacLachlan, C. (2017) An assessment of Indian monsoon seasonal forecasts and mechanisms underlying monsoon interannual variability in the Met Office GloSea5-GC2 system. *Climate Dynamics*, 48, 1447–1465. <https://doi.org/10.1007/s00382-016-3151-2>.
- Kaiser, J.W., Heil, A., Andreae, M.O., Benedetti, A., Chubarova, N., Jones, L., Morcrette, J.-J., Razinger, M., Schultz, M.G., Suttie, M. and van der Werf, G.R. (2012) Biomass burning emissions estimated with a global fire assimilation system based on observed fire radiative power. *Biogeosciences*, 9, 527–554. Available at: <https://www.biogeosciences.net/9/527/2012/>.
- Karmacharya, J., New, M., Jones, R. and Levine, R. (2016) Added value of a high-resolution regional climate model in simulation of intraseasonal variability of the south Asian summer monsoon. *International Journal of Climatology*, 37, 1100–1116.
- Keane, R.J., Williams, K.D., Stirling, A.J., Martin, G.M., Birch, C.E. and Parker, D.J. (2019) Fast biases in Indian summer monsoon rainfall in the Met Office unified model. *Journal of Climate*. <https://doi.org/10.1175/JCLI-D-18-0650.1>.
- Kettle, A.J., Andreae, M.O., Amouroux, D., Andreae, T.W., Bates, T.S., Berresheim, H., Bingemer, H., Boniforti, R., Curran, M.A.J., DiTullio, G.R., Helas, G., Jones, G.B., Keller, M.D., Kiene, R.P., Leck, C., Levasseur, M., Malin, G., Maspero, M., Matrai, P., McTaggart, A.R., Mihalopoulos, N., Nguyen, B.C., Novo, A., Putaud, J.P., Rapsomanikis, S., Roberts, G., Schebeske, G., Sharma, S., Simó, R., Staubes, R., Turner, S. and Uher, G. (1999) A global database of sea surface dimethylsulfide (DMS) measurements and a procedure to predict sea surface DMS as a function of latitude, longitude, and month. *Global Biogeochemical Cycles*, 13, 399–444.
- Kulkarni, J.R., Mahes Kumar, R.S., Morwal, S.B., Kumari, B.P., Konwar, M., Deshpande, C.G., Joshi, R.R., Bhalwankar, R.V., Pandithurai, G., Safai, P.D., Narkhedkar, S.G., Dani, K.K., Nath, A., Nair, S., Sapre, V.V., Puranik, P.V., Kandalgaonkar, S.S., Mujumdar, V.R., Khaladkar, R.M., Vijayakumar, R., Prabha, T.V. and Goswami, B.N. (2012) The cloud aerosol interaction and precipitation enhancement experiment (CAIPEEX): overview and preliminary results. *Current Science*, 102, 413–425. Available at: <http://www.jstor.org/stable/24083888>.
- Lamarque, J.-F., Dentener, F., McConnell, J., Ro, C.-U., Shaw, M., Vet, R., Bergmann, D., Cameron-Smith, P., Dalsoren, S., Doherty, R., Faluvegi, G., Ghan, S.J., Josse, B., Lee, Y.H., MacKenzie, I.A., Plummer, D., Shindell, D.T., Skeie, R.B., Stevenson, D.S., Strode, S., Zeng, G., Curran, M., Dahl-Jensen, D., Das, S., Fritzsche, D. and Nolan, M. (2013) Multi-model mean nitrogen and sulfur deposition from the atmospheric chemistry and climate model intercomparison project (ACCMIP): evaluation of historical and projected future changes. *Atmospheric Chemistry and Physics*, 13, 7997–8018. Available at: <https://www.atmos-chem-phys.net/13/7997/2013/>.
- Lean, H.W., Clark, P.A., Dixon, M., Roberts, N.M., Fitch, A., Forbes, R. and Halliwell, C. (2008) Characteristics of high-resolution versions of the Met Office unified model for forecasting convection over the United Kingdom. *Monthly Weather Review*, 136, 3408–3424.
- Levine, R.C. and Martin, G.M. (2018) On the climate model simulation of Indian monsoon low-pressure systems and the effect of remote disturbances and systematic biases. *Climate Dynamics*, 50, 4721–4743.
- Liss, P.S. and Merlivat, L. (1986) *Air–sea gas exchange rates: introduction and synthesis*. In: Buat-Ménard, P. (Ed.) *The Role of Air–Sea Exchange in Geochemical Cycling*, NATO ASI Series (Series C: Mathematical and Physical Sciences). Dordrecht: Springer, p. 185.
- Lock, A.P. (2001) The numerical representation of entrainment in parametrizations of boundary layer turbulent mixing. *Monthly Weather Review*, 129, 1148–1163.
- Lock, A.P., Brown, A.R., Bush, M.R., Martin, G.M. and Smith, R.N.B. (2000) A new boundary layer mixing scheme. Part I: scheme description and single-column model tests. *Monthly Weather Review*, 128, 3187–3199.
- MacLachlan, C., Arribas, A., Peterson, K.A., Maidens, A., Fereday, D., Scaife, A.A., Gordon, M., Vellinga, M., Williams, A., Comer, R.E., Camp, J., Xavier, P. and Madec, G. (2015) Global seasonal forecast system version 5 (GloSea5): a high-resolution seasonal forecast system. *Quarterly Journal of the Royal Meteorological Society*, 141, 1072–1084.
- Malcolm B. Senior Scientist. (Personal communication, November 2018).
- Mamgain, A., Rajagopal, E.N., Mitra, A.K. and Webster, S. (2018) Short-range prediction of monsoon precipitation by NCMRWF regional unified model with explicit convection. *Pure and Applied Geophysics*, 175, 1197–1218.
- MetOffice (2013) *Iris: A Python Library for Analysing and Visualising Meteorological and Oceanographic Data Sets*. Exeter: Met Office. Available at: <http://scitools.org.uk>.
- Mitra, A.K., Bohra, A.K., Rajeevan, M.N. and Krishnamurti, T.N. (2009) Daily Indian precipitation analysis formed from a merge of rain-gauge data with the TRMM TMPA satellite-derived rainfall estimates. *Journal of the Meteorological Society of Japan. Ser. II*, 87A, 265–279.
- Pearce, R.P. and Mohanthy, U.C. (1984) Onsets of the Asian summer monsoon 1979–82. *Journal of the Atmospheric Sciences*, 41, 1620–1639.
- Prakash, S., Mitra, A.K., Momin, I.M., Rajagopal, E.N., Milton, S.F. and Martin, G.M. (2016) Skill of short- to medium-range monsoon rainfall forecasts from two global models over India for hydro-meteorological applications. *Meteorological Applications*, 23, 574–586. <https://doi.org/10.1002/met.1579>.
- Rakhi, R., Jayakumar, A., Sreevathsa, M.N.R. and Rajagopal, E.N. (2016) *Implementation and up-gradation of NCUM in Bhaskara HPC*. Noida: National Centre for Medium Range Weather Forecasting (NCMRWF), Ministry of Earth Sciences. Technical Report NMRF/TR/03/2016. Available at: <https://doi.org/10.1314/RG.2.1.4624.7923>.
- Ramesh, K.J., Basu, S. and Begum, Z.N. (1996) Objective determination of onset, advancement and withdrawal of the summer monsoon using large-scale forecast fields of a global spectral model over India. *Meteorology and Atmospheric Physics*, 61, 137–151. <https://doi.org/10.1007/BF01025702>.
- Ramesh Kumar, M.R., Sankar, S. and Reason, C. (2009) An investigation into the conditions leading to monsoon onset over Kerala. *Theoretical and Applied Climatology*, 95, 69–82.
- Rao, P.C.S., Pai, D.S. and Mohapatra, M.E. (2017) *Monsoon 2016, a report*. Pune: National Climate Centre, India Meteorological Department. IMD Met. Monograph ESSO/IMD/SYNOPTIC MET/01(2017)/21
- Rawlins, F., Ballard, S.P., Bovis, K.J., Clayton, A.M., Li, D., Inverarity, G.W., Lorenc, A.C. and Payne, T.J. (2007) The Met Office global four-dimensional variational data assimilation scheme. *Quarterly Journal of the Royal Meteorological Society*, 133, 347–362.

- Smagorinsky, J. (1963) General circulation experiments with the primitive equations. *Monthly Weather Review*, 91, 99–164.
- Smith, R.N.B. (1990) A scheme for predicting layer clouds and their water content in a general circulation model. *Quarterly Journal of the Royal Meteorological Society*, 116, 435–460.
- Srivastava, A., Rao, S., Nagarjuna Rao, D., George, G. and Pradhan, M. (2017) Structure, characteristics and simulation of monsoon low-pressure systems in CFSv2 coupled model. *Journal of Geophysical Research: Oceans*, 122, 6394–6415.
- Stirling, A.J. and Stratton, R.A. (2012) Entrainment processes in the diurnal cycle of deep convection over land. *Quarterly Journal of the Royal Meteorological Society*, 138, 1135–1149.
- Stratton, R.A., Senior, C.A., Vosper, S.B., Folwell, S.S., Boutle, I.A., Earnshaw, P.D., Kendon, E., Lock, A.P., Malcolm, A., Manners, J., Morcrette, C.J., Short, C., Stirling, A.J., Taylor, C.M., Tucker, S., Webster, S. and Wilkinson, J.M. (2018) A pan-African convection-permitting regional climate simulation with the Met Office unified model: CP4-Africa. *Journal of Climate*, 31, 3485–3508.
- Stratton, R.A., Stirling, A. and Derbyshire, S. (2009) *Changes and Developments to Convective Momentum Transport (CMT) Parametrization based on Analysis of CRM and SCM*. Met R&D Technical Note 530. Exeter: Met Office.
- Turner, A.G., Bhat, G.S., Martin, G.M., Parker, D.J., Taylor, C.M., Mitra, A.K., Tripathi, S.N., Milton, S., Rajagopal, E.N., Evans, J.G., Morrison, R., Pattnaik, S., Sekhar, M., Bhattacharya, B.K., Madan, R., Govindankutty, M., Fletcher, J.K., Willetts, P.D., Menon, A., Marsham, J.H., Hunt, K.M., Chakraborty, T., George, G., Krishnan, M., Sarangi, C., Belušić, D., Garcia-Carreras, L., Brooks, M., Webster, S., Brooke, J.K., Fox, C., Harlow, R.C., Langridge, J.M., Jayakumar, A., Böing, S.J., Halliday, O., Bowles, J., Kent, J., O'Sullivan, D., Wilson, A., Woods, C., Rogers, S., Smout-Day, R., Tiddeman, D., Desai, D., Nigam, R., Paleri, S., Sattar, A., Smith, M., Anderson, D., Bauguutte, S., Carling, R., Chan, C., Devereau, S., Gratton, G., MacLeod, D., Nott, G., Pickering, M., Price, H., Rastall, S., Reed, C., Trembath, J., Woolley, A., Volonté, A. and New, B. (2019) Interaction of Convective Organisation with monsoon precipitation, atmosphere, surface and sea: the 2016 INCOMPASS field campaign in India. *Quarterly Journal of the Royal Meteorological Society*. <https://doi.org/10.1002/qj.3633>. [Accepted Author Manuscript].
- Turpin, B., Saxena, P. and Andrews, E. (2000) Measuring and simulating particulate organics in the atmosphere: problems and prospects. *Atmospheric Environment*, 34, 2983–3013.
- Vosper, S.B. (2015) Mountain waves and wakes generated by South Georgia: implications for drag parametrization. *Quarterly Journal of the Royal Meteorological Society*, 141, 2813–2827.
- Walters, D., Baran, A., Boutle, I., Brooks, M., Earnshaw, P., Edwards, J., Furtado, K., Hill, P., Lock, A., Manners, J., Morcrette, C., Mulcahy, J., Sanchez, C., Smith, C., Stratton, R., Tennant, W., Tomassini, L., Van Weverberg, K., Vosper, S., Willett, M., Browse, J., Bushell, A., Dalvi, M., Essery, R., Gedney, N., Hardiman, S., Johnson, B., Johnson, C., Jones, A., Mann, G., Milton, S., Rumbold, H., Sellar, A., Ujiie, M., Whitall, M., Williams, K. and Zerroukat, M. (2019) The Met Office Unified Model Global Atmosphere 7.0/7.1 and JULES Global Land 7.0 configurations. *Geoscientific Model Development*, 12, 1909–1963. <https://doi.org/10.5194/gmd-12-1909-2019>.
- Walters, D., Boutle, I., Brooks, M., Melvin, T., Stratton, R., Vosper, S., Wells, H., Williams, K., Wood, N., Allen, T., Bushell, A., Copsey, D., Earnshaw, P., Edwards, J., Gross, M., Hardiman, S., Harris, C., Heming, J., Klingaman, N., Levine, R., Manners, J., Martin, G., Milton, S., Mittermaier, M., Morcrette, C., Riddick, T., Roberts, M., Sanchez, C., Selwood, P., Stirling, A., Smith, C., Suri, D., Tennant, W., Vidale, P.L., Wilkinson, J., Willett, M., Woolnough, S. and Xavier, P. (2017) The Met Office Unified Model Global Atmosphere 6.0/6.1 and JULES Global Land 6.0/6.1 configurations. *Geoscientific Model Development*, 10, 1487–1520. Available at: <https://www.geosci-model-dev.net/10/1487/2017/>.
- Wang, B., Ding, Q. and Joseph, P.V. (2009) Objective definition of the Indian summer monsoon onset. *Journal of Climate*, 22, 3303–3316.
- Weusthoff, T., Ament, F., Arpagaus, M. and Rotach, M.W. (2010) Assessing the benefits of convection-permitting models by neighborhood verification: examples from MAP D-PHASE. *Monthly Weather Review*, 138, 3418–3433.
- Willett, M.R. and Whitall, M.A. (2017) *A simple prognostic based convective entrainment rate for the unified model: description and tests*. Exeter: Met Office. Technical Report 617
- Willetts, P.D., Marsham, J.H., Birch, C.E., Parker, D.J., Webster, S. and Petch, J. (2017b) Moist convection and its upscale effects in simulations of the Indian monsoon with explicit and parametrized convection. *Quarterly Journal of the Royal Meteorological Society*, 143, 1073–1085.
- Willetts, P.D., Turner, A.G., Martin, G.M., Mrudula, G., Hunt, K.M.R., Parker, D.J., Taylor, C.M., Birch, C.E., Mitra, A.K., Heming, J.T. and Brooks, M.E. (2017a) The 2015 Indian summer monsoon onset – phenomena, forecasting and research flight planning. *Weather*, 72, 168–175.
- Wilson, D.R., Bushell, A.C., Kerr-Munslow, A.M., Price, J.D. and Morcrette, C.J. (2008) PC2: a prognostic cloud fraction and condensation scheme. I: scheme description. *Quarterly Journal of the Royal Meteorological Society*, 134, 2093–2107.
- Wood, N., Staniforth, A., White, A., Allen, T., Diamantakis, M., Gross, M., Melvin, T., Smith, C., Vosper, S., Zerroukat, M. and Thuburn, J. (2014) An inherently mass-conserving semi-implicit semi-Lagrangian discretization of the deep-atmosphere global non-hydrostatic equations. *Quarterly Journal of the Royal Meteorological Society*, 140, 1505–1520.
- Woodhams, B.J., Birch, C.E., Marsham, J.H., Bain, C.L., Roberts, N.M. and Boyd, D.F.A. (2018) What is the added value of a convection-permitting model for forecasting extreme rainfall over tropical East Africa?. *Monthly Weather Review*, 146, 2757–2780. <https://doi.org/10.1175/MWR-D-17-0396.1>.
- Xavier, P.K., Marzin, C. and Goswami, B.N. (2007) An objective definition of the Indian summer monsoon season and a new perspective on the ENSO–monsoon relationship. *Quarterly Journal of the Royal Meteorological Society*, 133, 749–764.

## SUPPORTING INFORMATION

Additional supporting information may be found online in the Supporting Information section at the end of this article.

**How to cite this article:** Martin GM, Brooks ME, Johnson B, et al. Forecasting the monsoon on daily to seasonal time-scales in support of a field campaign. *Q J R Meteorol Soc.* 2019;1–22. <https://doi.org/10.1002/qj.3620>

## APPENDIX: DETAILS OF SIMPLIFIED CLASSIC AEROSOL SCHEME

The simplified version of CLASSIC used here includes all species listed in section 2 except for sea salt. A further simplification is that all primary emissions of carbonaceous aerosol (fossil fuel, biofuel, biomass burning) are lumped into one carbonaceous aerosol species. The physical and optical properties of the lumped carbonaceous aerosol species follow those used in CLASSIC for biomass-burning aerosols. This simplification will lead to an underestimation of solar absorption by the aerosol (overestimation of single-scattering albedo), as the ratio of black carbon (BC) to organic carbon (OC) assumed in the biomass-burning aerosol (BBA) species is much lower than the typical ratio of BC:OC simulated by CLASSIC when comparing the aerosol mass from soot and OC species. By using the BBA species for the lumped carbonaceous aerosol, there are also some increases in AOD relative to treating them separately. This is because BBA are assumed to grow during ageing (mass increases by a factor of 1.62), whereas this is not assumed for the soot and OC species. The specific extinction coefficient and hygroscopic growth are very similar for organic carbon and BBA species in CLASSIC with dry values of around  $5 \text{ m}^2/\text{g}$ . In summary, although the optical properties (particularly absorption) will not be well approximated in the lumped carbonaceous aerosol scheme, the spatial distribution of AOD and aerosol mass, particularly in BB-dominated regions, will be well approximated.

In addition to the lumped carbonaceous aerosol species, the full sulphur cycle and sulphate aerosol representation from CLASSIC were included. The two-bin dust scheme was also included, with data assimilation from MODIS Aqua Collection 5.1 deep blue and dark target algorithms (Malcolm Brooks, personal communication, November 2018). Because the data assimilation was shown to lead to an overestimation of dust AOD over some land areas, a regional and time-varying dust tuning factor was applied. The tuning factor for Southern Asia was 0.47 at T+0, rising linearly to 0.98

at T+144, based on calibrating the modelled total AOD to MODIS observations.

Stratospheric aerosol was represented via the climatology from Cusack *et al.* (1998). Secondary organic aerosol (SOA) is not modelled explicitly by CLASSIC, but the contribution to AOD and radiative effects is included using an offline climatology. The SOA climatology is provided by the UK Met Office Chemistry Transport Model (STOCHEM: Derwent *et al.*, 2003) based on the emission of isoprene from biogenic sources.

BBA emissions were taken from the Global Fire Assimilation System (GFAS: Kaiser *et al.*, 2012). The “total carbon” emission factor was used to provide the total aerosol mass emission for CLASSIC. This neglects the conversion of organic carbon (carbon mass only) into the full mass of primary organic matter. Typically, POM:OC ratios of freshly emitted carbonaceous aerosol (both smoke and urban emissions) are in the range 1.4–1.7 (Turpin *et al.*, 2000; Aiken *et al.*, 2008). However, CLASSIC scales up BBA mass by a factor of 1.62 during ageing (fresh aerosol is converted to aged aerosol on a 6-hr *e*-folding time-scale). The inclusion of this ageing process more or less compensates for omitting the conversion of OC emissions to POM.

Anthropogenic emissions of  $\text{SO}_2$  and carbonaceous aerosol (from fossil fuel and biofuel) for both aerosol schemes were based on the year 2014 monthly mean emissions MACC/CityZEN (via ECCAD-Ether at <http://eccad.sedoo.fr>). The MACC/CityZen emissions are based on an interpolation from the historical emissions for 2000 from ACCMIP (Lamarque *et al.*, 2013), with some regional updates to these emissions in 2005 and 2010 from the RCP8.5 scenario (Granier *et al.*, 2011; Diehl *et al.*, 2012). As with GFAS, no scaling from OC to POM was used for the fossil-fuel or biofuel emissions. Volcanic degassing emissions of  $\text{SO}_2$  were taken from Andres and Kasgnoc (1998). Emissions of dimethyl sulphide (DMS) were calculated from the Kettle *et al.* (1999) ocean DMS climatology with the Liss and Merlivat (1986) surface-exchange parametrization.